Exponential distribution of wave-driven near-bed water speeds under short-crested waves: a case study in the eastern Gulf of Riga, the Baltic Sea

Maris Eelsalu[a1] [ID], Laura Piho[b1] [ID], Juris Aigars[c] [ID],
Loreta Kelpšaitė-Rimkienė[d] [ID], Vitalijus Kondrat[d] [ID],
Maarja Kruusmaa[b] [ID], Kevin E. Parnell[a] [ID], Asko Ristolainen[b] [ID],
Ilona Šakurova[d] [ID], Māris Skudra[c] [ID], Maija Viška[c] [ID] and
Tarmo Soomere[a,e] [ID]

[a] Wave Engineering Laboratory, Department of Cybernetics, School of Science, Tallinn
   University of Technology, Ehitajate tee 5, 19086 Tallinn, Estonia
[b] Center for Biorobotics, School of Information Technologies, Tallinn University of
   Technology, Ehitajate tee 5, 19086 Tallinn, Estonia
[c] Latvian Institute of Aquatic Ecology, Voleru iela 4, Kurzemes rajons, LV-1007 Rīga, Latvia
[d] Marine Research Institute, Klaipėda University, Herkaus Manto g. 84, 92294 Klaipėda,
   Lithuania
[e] Estonian Academy of Sciences, Kohtu 6, 10130 Tallinn, Estonia

ABSTRACT

Loads exerted to the seabed by short-crested wind-seas with a wide directional spread have
extensive spatio-temporal variability. We quantify this variability in terms of near-bed water
speed using an array of nine high-resolution hydromast devices for recording pressure and
water velocity in the range of 0.12–1 m/s mounted at a distance of 10 m from each other on a
rigid rectangular frame of 20 × 20 m in approximately 4 m deep water and 700 m from the
eastern shore of the Gulf of Riga near Skulte (Latvia) in August–September 2022. This array is
complemented by an acoustic Doppler velocimeter (ADV). The average background current is
very weak, approximately 0.003 m/s in the measurement location. The empirical distributions
of velocity components are symmetric but greatly deviate from the expected Gaussian
distribution. The empirical distributions of water speeds follow an exponential distribution rather
than a Rayleigh or Forristall distribution. This shape of the distributions appears in the range of
0.2–0.7 m/s while the maximum speed reaches 1.22 m/s. The rate parameter (inverse scale
parameter) varies almost by a factor of two in recordings by different devices. The recordings
make it possible to identify wakes of vessels entering to or departing from the Port of Skulte.

Introduction

Wave-driven loads in the nearshore and at the shore are usually extremely variable
and may seriously damage even the most stable coastal engineering structures (Poncet
et al. 2022; Ma et al. 2023). Even nominally identical and long-crested waves often
produce very different spatial and temporal pressure distributions on the structure
(Bullock et al. 2007). It is likely that this variability is even more pronounced when
waves are short-crested. This is a typical situation in wind-seas with wide directional
spread of wave energy. This sort of variability also becomes evident in terms of near-
bottom velocities and associated hydrodynamic loads in the nearshore of areas that
often host short-crested wave conditions.

It is well known that turbulent kinetic energy under shoaling and breaking waves
(i) exhibits large temporal variations, (ii) is different for spilling and plunging breakers
and (iii) does not show any clear dependence on the wave parameters even under
long-crested ocean waves (Christensen et al. 2019; Aagard et al. 2021). Zhai et al.
(2022) showed that long-crested wave models can overestimate the ability of break-
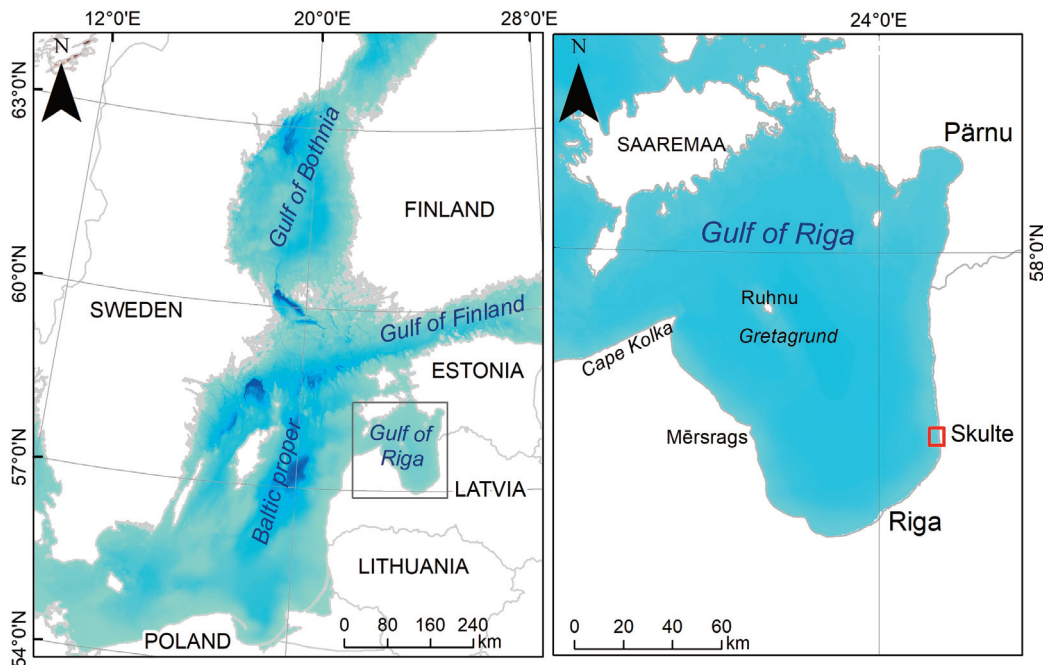waters to protect the structures in a short-crested sea. The presence of short-crested

---

[1] Shared first authors, maris.eelsalu@taltech.ee, laura.piho@taltech.ee

Fig. 1. Map of the location of near-bottom velocity measurements in the nearshore of the eastern coast of the Gulf of Riga near Skulte, Latvia.

waves may lead to an increase in near-bottom velocities (Zheng et al. 2006).

The Baltic Sea (Leppäranta and Myrberg 2009) and even more so its large sub-basins have a wave climate in which active, usually short-crested wind-seas predominate, and the proportion of regular long-crested swells is low (Broman et al. 2006; Björkqvist et al. 2021). It is therefore likely that the fields of wave-generated near-bottom velocities have commonly much larger variability than similar fields produced under regular swell conditions. This feature may play a particularly important role in driving coastal processes, first of all in terms of entrainment of finer bottom sediments into the water column and local mobility of sediment in patches impacted by higher examples of wave loads. To take this feature into account, it is necessary to systematically quantify this variability in time and space. To a first approximation, this can be done in terms of properties of the occurrence probability of different wave-induced velocities in the nearshore. These properties are necessary to reach adequate estimates of spatial variations in the largest loads that play a crucial role in the initiation of particle movement under turbulent flow conditions (Diplas et al. 2008). These loads generally follow the properties of the highest water speed values. Their description is usually built using extreme value distributions. The relevant techniques require that the underlying data (e.g. water speed maxima over certain time intervals) follow the same probability distribution (e.g. Coles 2004).

The main aim of this research was to achieve a better understanding of the appearance of near-bottom flow velocity distributions and their spatial variations under short-crested waves, with particular emphasis on statistical properties of wave-driven higher flow speeds. We did not make any attempt to separate purely wave-driven motions from other motion components. This would be possible using, for example, the empirical mode decomposition technique (Huang et al. 1998; Bian et al. 2020). This task was addressed by

means of field experiments in the eastern nearshore of the Gulf of Riga (Fig. 1).

The main properties of the wave climate in the Gulf of Riga were evaluated, to a first approximation, by Eelsalu et al. (2014) using historical visual wave observations. They were further analysed in Najafzadeh et al. (2024) using the SWAN model forced by ERA5 winds for the time period of 1990–2021. Waves in this basin are usually governed by the local winds and are mostly locally generated. The wave climate in the entire gulf is relatively mild. The long-term average wave height is mostly in the range of 0.7–0.8 m. Wave periods are predominantly 2–5 s. Wave fields are usually fully saturated wind-seas. The northern part of the gulf occasionally contains low swells generated in the Baltic proper. The modelled significant wave height reached well over 4 m in the gulf's entire eastern part during the January 2005 storm Erwin/Gudrun (Najafzadeh et al. 2024) and may have exceeded 6 m in an extreme storm in 1967 (Björkqvist et al. 2018). The wave climate is milder in the western part of the gulf and more severe in the eastern nearshore.

The presented features suggest that the eastern nearshore of the Gulf of Riga is frequently affected by wind-seas with a wide directional spectrum. In other words, this is a suitable region for studies of specific features of short-crested wave systems. We used an array of nine sensors to estimate spatial variability in the wave-driven bottom velocity field. The recordings were carried out with the Hall effect sensor-based velocity and direction estimation devices called hydromasts (Ristolainen et al. 2019; Egerer et al. 2024). The devices were mounted on a regular rectangular grid with a step of 10 m. This distance is large enough to detect spatial variations in the near-bottom velocity field. The hydromasts were complemented by a Nortek Acoustic Doppler Velocimeter (ADV).

In this paper, we describe the main features of wave-driven velocity fields extracted from the high-resolution measurements of near-bottom velocities in the nearshore of

Table 1. Thresholds for adequate velocity recordings for hydromasts H01–H09 (Fig. 12), percentage of speed recordings exceeding four thresholds, maximum recorded speed, parameters of a Weibull distribution approximation of the rebuilt distributions for water speed, and an estimate of the rate parameter based on empirical distributions of water speeds in the range of 0.25–0.875 m/s. Water depth in the location of the hydromasts is evaluated from the pressure sensor of the hydromasts

Hydromast	Depth, m	Threshold, m/s	Percentage of speed recordings exceeding the indicated speed threshold, m/s				Maximum speed, m/s	Parameters of Weibull distribution		Rate parameter
			Threshold	0.15	0.3	0.5		k	λ	A
H01	4.061	0.1175	5.10	2.36	0.41	0.045	0.933	1.1125	0.0504	11.8
H02	4.056	0.1025	11.04	5.24	1.31	0.23	1.042	0.8991	0.0525	8.6
H03	4.064	0.1075	12.15	7.09	1.69	0.39	1.164	0.8460	0.0545	7.08
H04	4.063	0.1025	6.93	2.70	0.48	0.052	1.028	1.0710	0.0491	11.5
H05	4.048	0.1025	11.77	5.69	1.78	0.40	1.143	0.8383	0.0527	7.5
H06	4.060	0.1075	12.70	6.82	1.86	0.38	1.111	0.8571	0.0557	8.0
H07	4.030	0.1075	7.49	3.51	0.85	0.13	1.032	0.9716	0.0502	9.9
H08	4.061	0.1125	5.00	2.51	0.485	0.053	1.055	1.0800	0.0494	12.2
H09	4.060	0.1075	8.14	3.31	0.865	0.18	1.217	0.9552	0.0502	7.9
ADV	–	–	–	8.22	2.09	0.36	1.162	1.16	0.0584	–

the Gulf of Riga. The description focuses on the appearance and parameters of the empirical distributions of near-bottom water velocities. The presentation starts with a description of the study site, wave properties in the study area during the experiment, the devices used, their configuration and procedures for pre-processing the raw data. To make the presentation compact and still unambiguous, we employ the notion in which 'velocity' is understood as a vector, with its components possibly having negative values, while 'speed' means the magnitude (of velocity) and is always non-negative. The analysis of water velocities, their variability and intermittency shows that the background current is very weak at the measurement location, empirical distributions of velocity components and water speeds only partially follow their usual (normal and Rayleigh) distributions, and that hydromasts are reliable also beyond their guaranteed measurement range. Finally, the outcome of this preliminary analysis is set into a wider context.

Study site and devices

Study site and meteorological conditions

The location of the measurements is near Skulte in the eastern Gulf of Riga and is expected to reflect the typical wave conditions in this gulf under the most frequent south-western and less frequent north-north-western winds (Soomere 2003; Männikus et al. 2023). The Gulf of Riga is the third largest semi-enclosed sub-basin of the Baltic Sea, with a surface area of 17 913 km^2, that is, approximately 5% of the entire Baltic Sea. It has a generally regular, oval-like shape and mostly smooth bathymetry, with dimensions approximately 130 × 140 km in the west-east and south-north direction, and the average and maximum depths of 21 and 52 m, respectively (Suursaar et al. 2002). The nearshore of the western, southern, and eastern coasts of the gulf has its 10 m isobath located approximately 2 km from the shore and the 20 m isobath roughly 3.5–8 km from the shore. These isobaths are almost parallel to the shoreline, and the nearshore can be adequately approximated by an inclined plane. Only the northern and north-eastern segments of the gulf are less regular (Fig. 1). The island of Ruhnu and a seabed elevation,

Gretagrund, are located near the geometric centre of the gulf. This layout of the gulf means that the impact of refraction on wind wave propagation is comparatively small in most of the gulf and that wave properties in the nearshore largely reflect those that exist farther offshore (Najafzadeh et al. 2024), with possible modifications owing to refraction and shoaling over the plane geometry.

The devices were mounted at 57°19'16.6" N, 24°23'33.8" E (Fig. 2) approximately 500 m from the shore near the seaward border of the gently sloping nearshore area from 2 August to 8 September 2022. The water depth at the location (approximately 4 m) was slightly shallower than the closure depth in this particular area (that is, the depth down to which wind waves maintain a specific type of coastal profile, this depth being approximately 4.5 m in the study area; Soomere et al. 2017). The seabed around the devices is therefore only occasionally affected by breaking high waves that may bring large amounts of finer sediment into motion and, ideally, shape the equilibrium profile down to the closure depth. The seabed was almost horizontal in the location of the frame: the average water depth along the sides and in the centre of the frame varied in the range of 4.030–4.064 m (Table 1).

The usual wave-driven alongshore sediment transport direction along the eastern shore of the Gulf of Riga is to the north, but reversals of this transport occur often in the vicinity of the study area (Viška and Soomere 2013). The entrance channel of the Port of Skulte, approximately 400 m to the south of the location of the devices, is 8–9 m deep and thus largely cuts sediment transport to the north. It is therefore natural that the vicinity of the measurement location suffers from the deficit of finer sediment. As the seabed in this area contains a very limited amount of fine sediment and is mostly covered by gravel, the equilibrium beach profile is not formed in this location. The seabed is generally smooth and very gently sloping. It contains a slightly deeper trench at a distance of 200–400 m from the shore and many small variations in water depth (Fig. 2). The typical height of bedforms is approximately 10 cm for single stones and 20–40 cm for larger elevations and depressions. There are no steep scarps. As the beach is mostly low-angle, a very small amount of reflected wave energy reaches the measurement location.
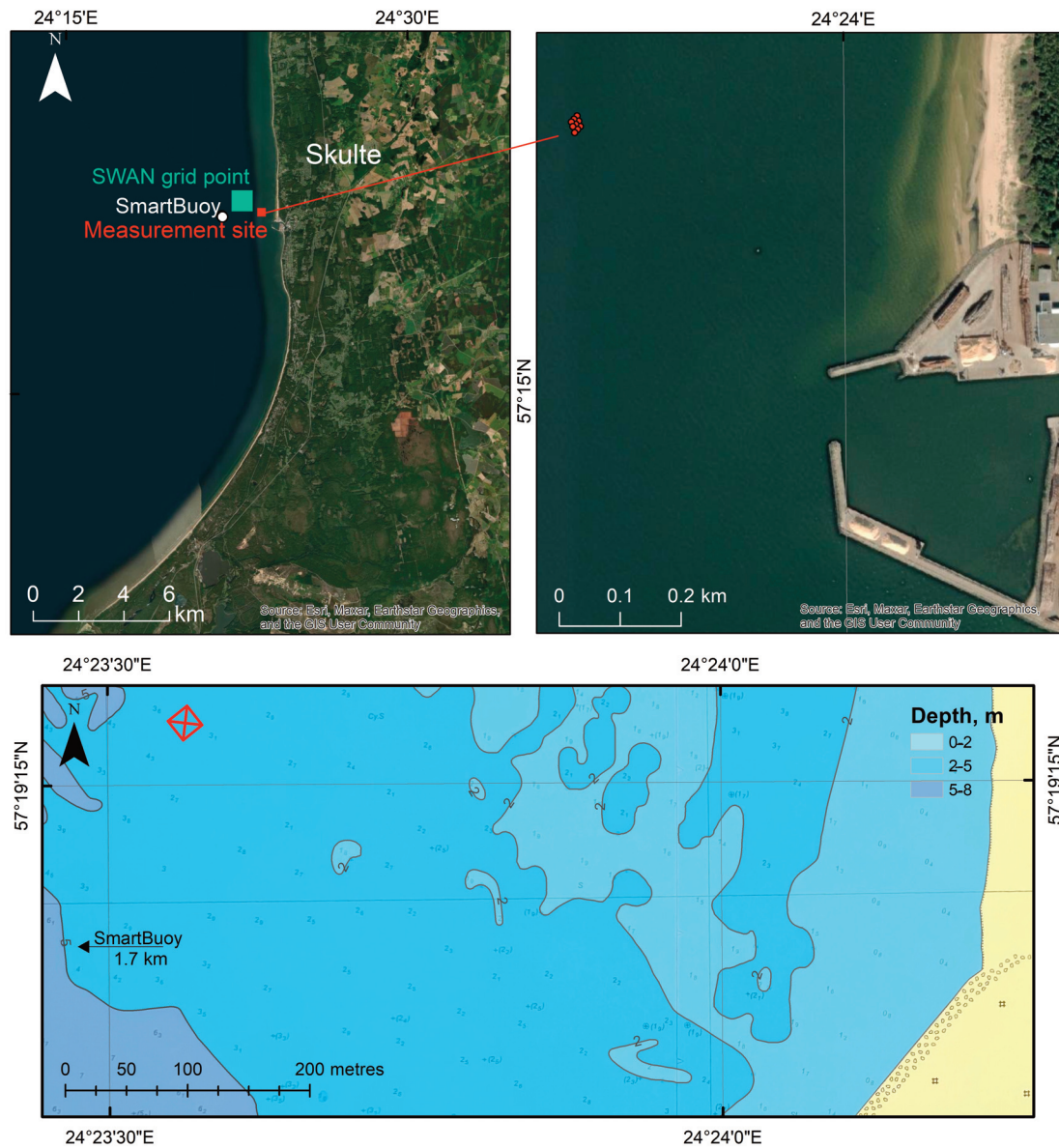
Fig. 2. Detailed map of the study location in the Gulf of Riga near Skulte, Latvia (upper panels) and showing the orientation of the frame (red square, lower panel).

Wave properties during the experiment were recorded by a SmartBuoy once an hour near the Port of Skulte at 57°19.199' N and 24°21.813' E at water depth of 15 m at a distance of approximately 1.5 km from the experiment site (Fig. 2). Wave data were acquired using a Wave and Tide Sensor 5218 (Aanderaa, Norway). The estimates of wave heights were based on the pressure time series measured over 120 s. The device also measured speed and direction of currents using a single-point ZPulse® Doppler Current Sensor 4420 (Aanderaa, Norway) with a resolution of 0.1 mm/s and 0.01°. Both sensors were connected to a SmartGuard measurement system. In our study, we only used the wave data from these devices.

The time interval of 120 s used for the evaluation of wave properties by the SmartBuoy is much shorter than commonly applied intervals (15–20 min) in the analysis of ocean waves and may lead to a short-time over- or underestimation of wave heights. For this reason, we also incorporated modelled wave properties from simulations using a multi-nested SWAN model (Giudici et al. 2023), applied to the Gulf of Riga with

a spatial resolution of 1 nautical mile (Najafzdeh et al. 2024). The wave parameters were extracted from a grid cell at 24°22'48" E, 57°19'30" N, water depth 8.6 m, located approximately 600 m from the measurement location (Fig. 2).

The modelled significant wave height (SWH) fluctuated around the long-term average of 0.5 m in July and reached 0.8 m on 7 August, a few days after the commencement of the measurements (Fig. 3). The rest of August was almost calm, with the SWH approximately 0.2 m and only one short event with SWH up to 0.4 m on 24 August. Somewhat higher waves, with SWH up to 1 m, occurred at the very end of August and on the last days of the experiment, whereas the SWH fluctuated around 0.4 m in the period of 1–6 September. Short single peaks in the SmartBuoy wave height recordings likely resulted from the short time interval of tracking the sea surface.

The waves predominantly arrived at the measurement location from the west and west-north-west, with a few short events with waves from the north (Fig. 3). Easterly winds predominated during the very calm time from 7 August until the end of the month when the waves were propagating in
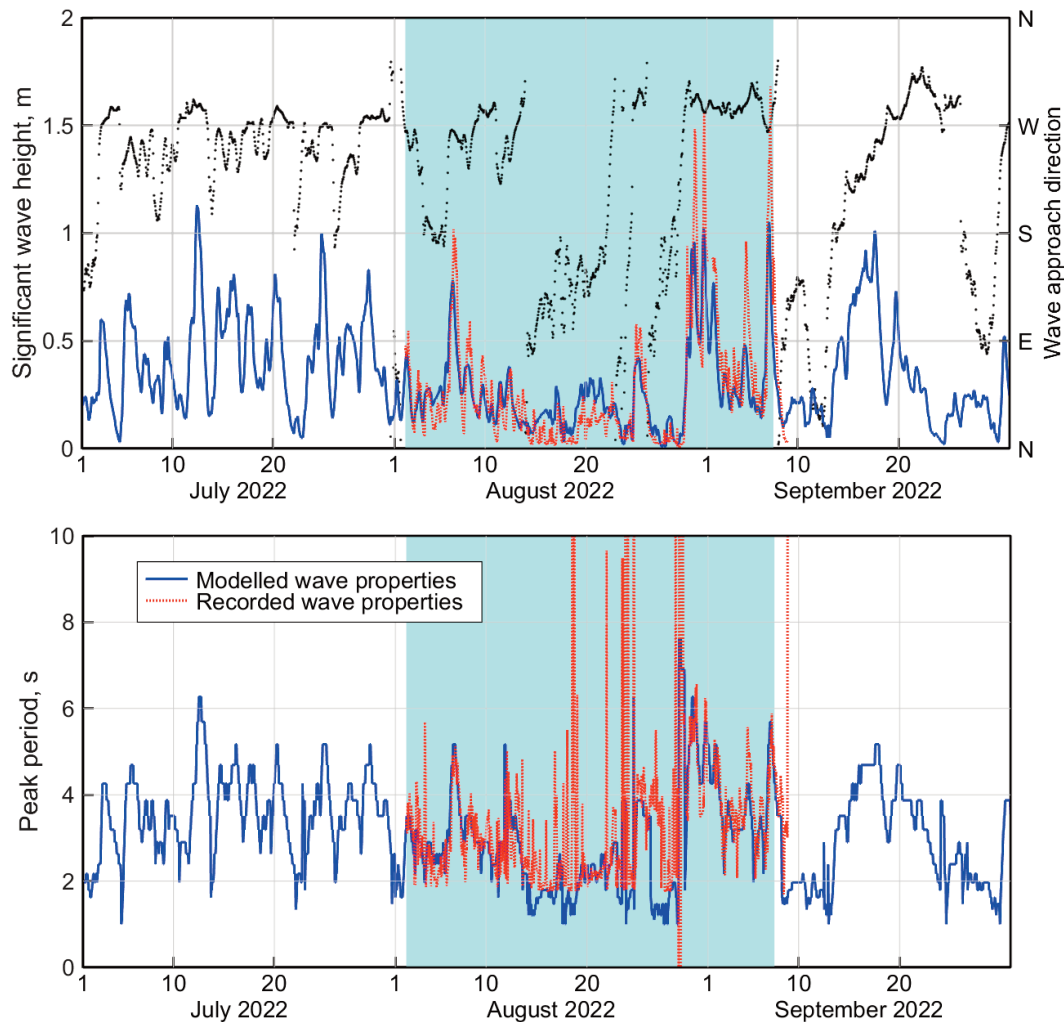
Fig. 3. Measured and modelled wave properties in the vicinity of the experiment site in July–September 2022. Black dots in the upper panel represent modelled wave directions. Light blue shading indicates the time period of the measurements. A few very large peak periods (red peaks on the lower panel) evaluated by the SmartBuoy reach 14–18 s. They occur during very low wave heights (<0.1 m) and may represent low long-period waves generated in remote regions of the Baltic proper, or may be an artifact of the analysis for very small waves.

the offshore direction. During stronger wave events in September, waves arrived either from the north-north-west or south, on some occasions probably under rapidly rotating wind conditions. The wave periods mostly fluctuated between 2 and 4 s and largely followed the course of wave heights. The periods were larger, up to 6 s at the end of August when the waves arrived from north-north-west, that is, from the direction of the longest fetch for the experiment site.

Devices

For measuring near-bottom water velocities, we used an acoustic Doppler velocimeter (ADV) (Nortek Vector) that records all three velocity components, along with nine devices known as 'hydromasts' (Ristolainen et al. 2016). This device was designed to distinguish rapidly changing near-bed hydro-dynamic loads in rivers. The name stems from a common nick-name for a specific organ of the lateral line of the fish that is capable of sensing the flow of water around it (Bleckmann and Zelick 2009). The device records absolute pressure (including its rapid fluctuations) and a proxy of water velocity (that is, both speed and direction; Ristolainen et al. 2019).

The hydromasts used in this study (Fig. 4) encompass a 300 mm long, 15 mm diameter polycarbonate hollow vibrat-

ing mast, covered with biofouling resistive copper tape, that reacts to vortices and other small fluctuations in the flow (Egerer et al. 2024). The vibrations of the mast are registered by measuring the rotation of a cylindrical 5 × 5 mm neody-mium magnet (fixed into the lower end of the mast) with a 3D Hall sensor (TLV493D-A1B6, Infineon Technologies AG; Fig. 4) inside the body of the hydromast. The validated velocity range is from 0.15 to 1.0 m/s (Egerer et al. 2024).

A stationary inertial measuring unit (IMU) (LSM6DS3TR-C + LIS3MDL - Precision 9 DoF IMU, Adafruit Industries LLC) was used for installation reference, background motion detection and for installation heading estimation. An absolute pressure sensor (MS5837, TE Connectivity, pressure range 0–2 bar) was used to record pressure changes over the device. The hydromasts were used in offline mode in this study, meaning that the raw data were stored locally, continuously using Feather M0 Addalogger (Adafruit Industries LLC) with a real time clock at the rate of 50 Hz. The orientation of the device was detected using an onboard compass BNO055 (Bosch Sensortec GmbH). A nine-cell alkaline battery pack was used to power the device, allowing measurements up to 45 days. The total weight of the device is around 1.4 kg.
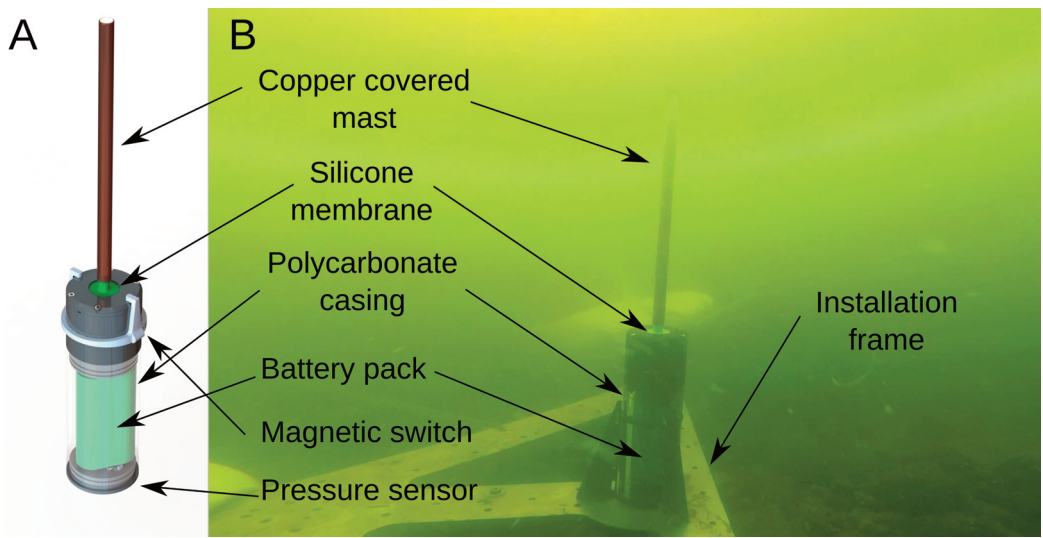
Fig. 4. A – components of the hydromast, B – the working device.

The time stamps of all hydromasts were aligned using an electromagnetic synchronisation coil before and after the experiments. The post-processing included water speed estimation, calculation of velocity direction and removal of the atmospheric pressure offset. The background information about atmospheric conditions was recorded using a HOBO pressure logger (HOBO U20-001-01, Onset Computer Corporation) that sampled atmospheric pressure at 15 min intervals.

The frame

Nine hydromasts used in the experiment and referred to as H01–H09 were assembled into a regularly spaced rectangular array using a 20 × 20 m aluminium frame (Fig. 5). The distance between the closest hydromasts was 10 m. The time-average water depth at the measurement site was 4 m. The frame was towed to the measuring site by floating buoys, lowered to the seabed by releasing them one side at a time and anchored to the seabed by divers using 20 kg sandbags between the sensor nodes. The measuring points of the hydromast masts (centre of the mast) were at the height of 0.45 m. The absolute pressure used for estimates of the water depth was read at a height of 0.05 m above the seabed. This composition minimised the probability of silting and scour around the devices and thus mechanical fouling owing to deposits of
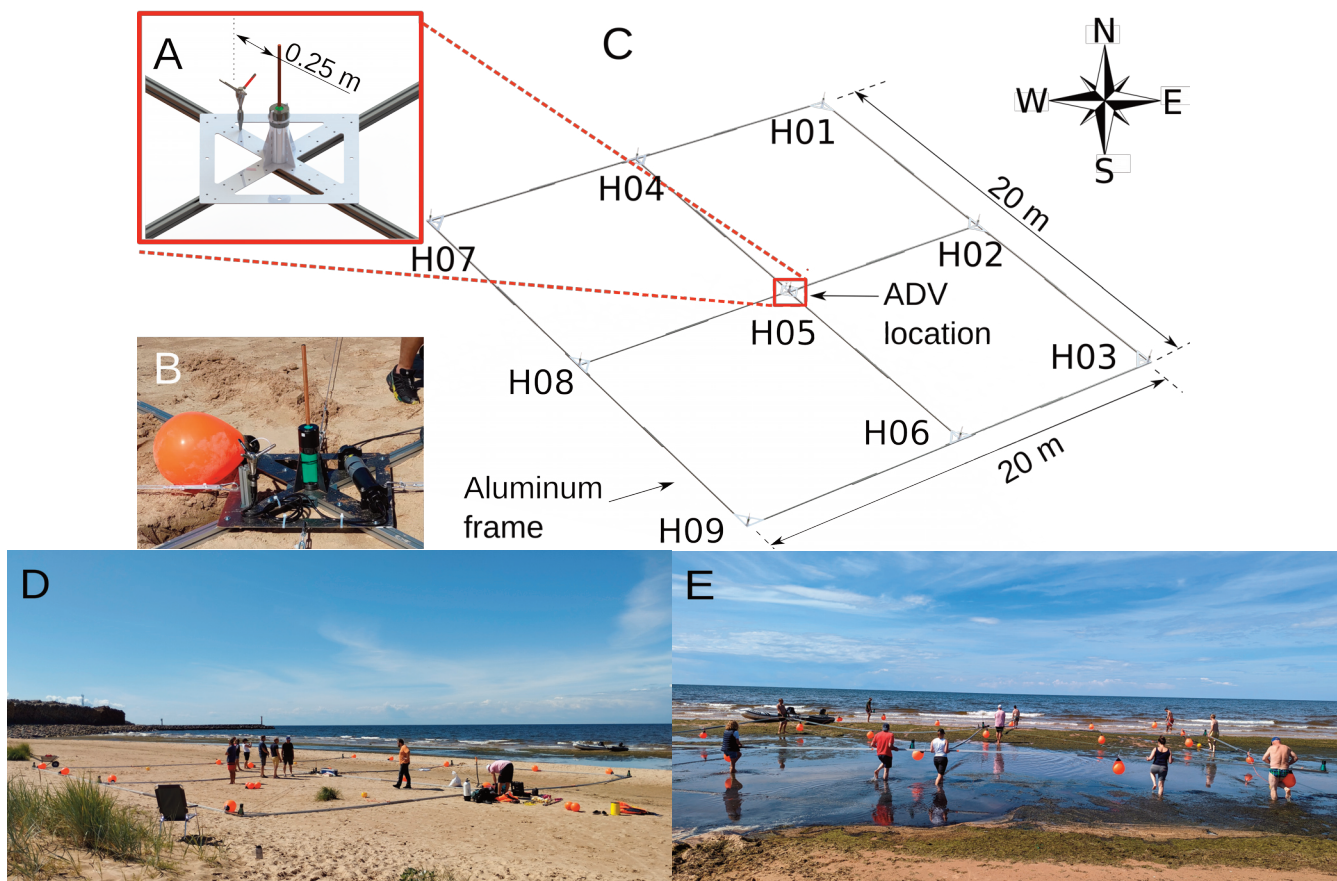

Fig. 5. The mounting frame for the hydromasts: A – placement of the ADV in reference to the central hydromast H05, B – mounted hydromast with the ADV, C – overview of the frame and locations of hydromasts H01–H09, D – assembly on the coast, E – the frame being carried to the sea. Photos by Centre of Biorobotics, Tallinn University of Technology.

fine sediments on the moving part of the device. The velocity recordings at the height of the measuring point are only very little affected by boundary layer effects.

An ADV was mounted pointing upwards adjacent to sensor H05 in the centre of the experimental frame and the hydromast array (Figs 4 and 5). The sampling volume, located approximately 0.4 m above the seabed, was at a level approximately equal to the middle of the hydromast's vibrating mast. The ADV data were sampled at 8 Hz for two-minute bursts (960 samples) every half an hour during the entire measurement period.

All devices were oriented with respect to the latitude-longitude coordinate system to record separately the west-east (denoted as the *u*-component, latitudinal or zonal velocity, positive to the east) and south-north (*v*-component, longitudinal or meridional velocity, positive to the north) components of water velocity. As the shoreline in the study area is oriented almost exactly in the south-north direction, the *u*-component reflects the cross-shore velocity and the *v*-component the alongshore velocity. The notion 'ADV-recorded water speed' means horizontal speed evaluated from the *u*- and *v*-components. Additionally, the ADV recorded the vertical velocity component.

The frame was installed on 2 August and retrieved on 8 September of 2022. The data were thus gathered in total for 37 days. Part of the 2 August data were discarded due to the only motion present being during the installation. The 8 September hydromast data were discarded as six out of nine hydromasts had stopped recording before the recovery. H01 and H04 had the last data from 6 September. H02, H03, H06 and H08 recorded until 7 September. Only H05, H07 and H09 recorded until 8 September; however, they stopped during the early hours before the recovery. For the listed reasons, the hydromast data from 3 August to 7 September are used in the analysis below.

Pre-processing of raw data

The data were first filtered and spurious data spikes removed. The ADV data set contained 1826 bursts. The records during the first bursts and during the last 46 bursts represent the situation before deployment and after recovery from the bottom and are thus discarded. Burst No. 1776 contained a high velocity peak approximately 1 m/s on the background of motions of 0.05 m/s. It may contain a signal of a vessel, but more likely, it reflects another disturbance. For this reason, bursts Nos 1776–1780 are also excluded from the analysis.

The remaining bursts showed very small residual motion –0.0030 m/s in the west-east direction, 0.0028 m/s in the south-north direction. Almost zero residuals of both velocity components apparently mirror the very weak average current in the measurement site. As expected, the average vertical velocity is zero with four significant digits (0.0000). The overall average horizontal flow speed was 0.0630 m/s. The vertical velocity component added approximately 2% to the total flow speed of 0.0644 m/s.

The ADV data were then upsampled to account for the different sampling rates. Because the clocks of the ADV and hydromasts were offset, the records were aligned by shifting the ADV record to achieve the highest correlation of pressure records within a time window, with the shift being typically around 25 s. Using this process, very good matches were achieved for both pressure and velocity data (Figs 6–8). On rare occasions a reliable match was not achieved. Such occasions were typically under very low wave energy conditions when an almost constant flow speed recorded by the hydromasts did not adequately represent the situation (see Section 'Matching ADV and hydromast data'), and pressure data of the hydromasts were dominated by noise.

For a few data bursts in the second half of the experiment, most of the burst for both pressure and velocity aligned well using the method described, but the pressure data for the first part of the burst (up to the first one-third) did not match. We therefore assume we achieved the correct time alignment but that there was a problem with the pressure recording. The reason for this remains unclear; however, we note that these events only occurred at times when there were large and reasonably rapid water temperature fluctuations, so it may be that the ADV took some time to adjust to the changed en-
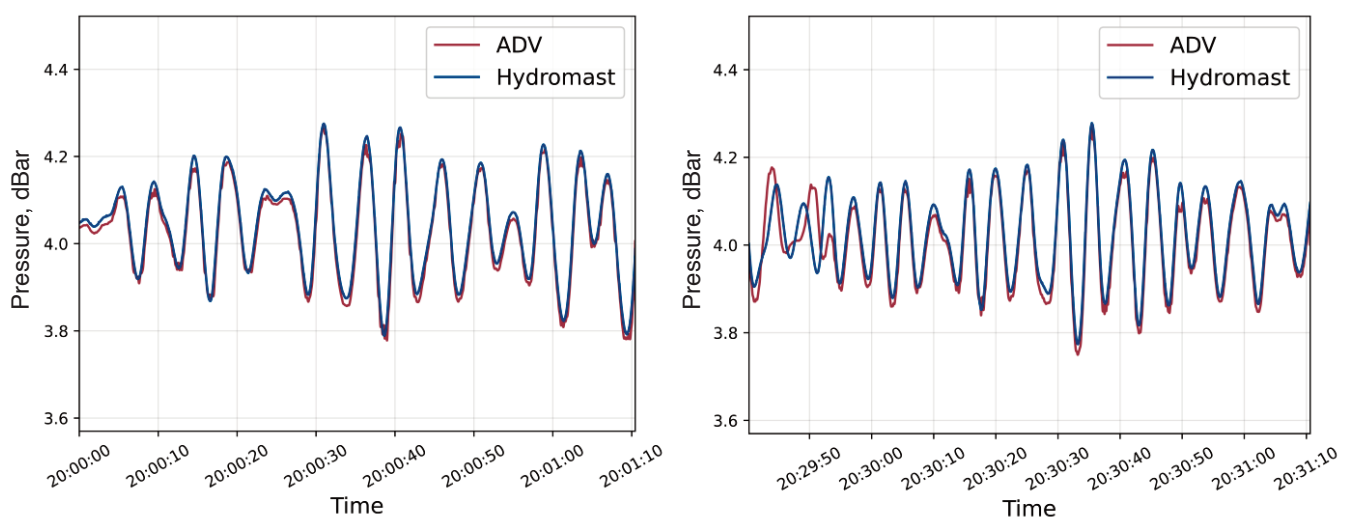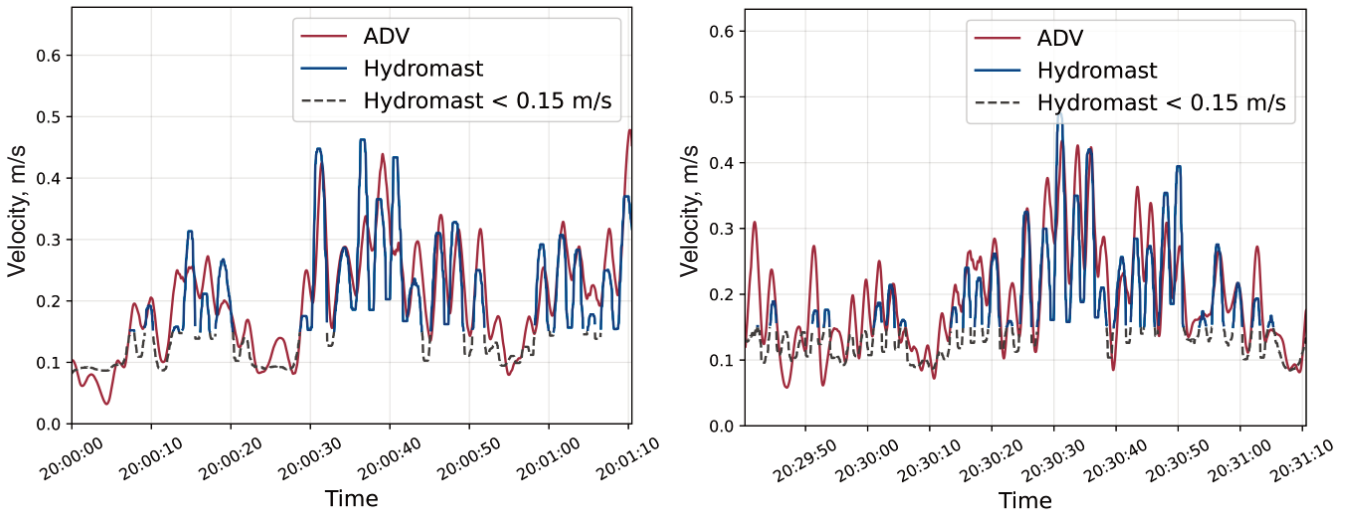

Fig. 6. Timing of water pressure registered using hydromast H05 (Fig. 5) and the ADV. The image at left starts at 20:00 and at right – at 20:30 EEST on 31 August 2022. The horizontal axis represents the hydromast sampling rate where 1 s corresponds to 50 sampling points.

Fig. 7. Timing of raw recordings of water speed registered using hydromast H05 (Fig. 5) and the ADV. See a more exact description of the data in the caption of Fig. 6. The procedure of eliminating potentially inadequate water speed recordings is described in Section 'Matching ADV and hydromast data'.
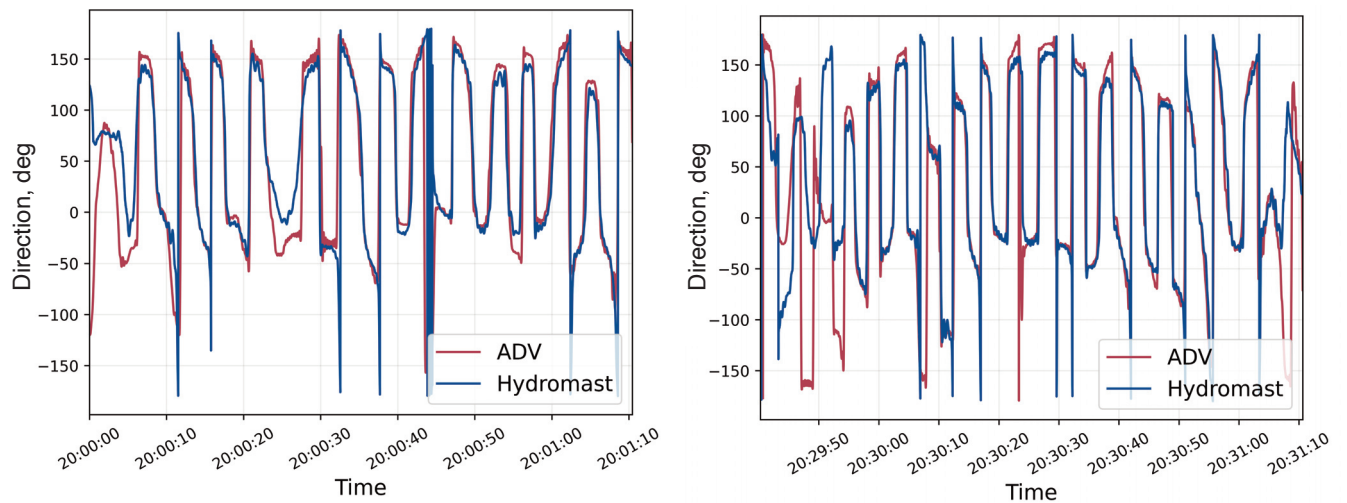
Fig. 8. Timing of flow direction registered using hydromast H05 (Fig. 5) and the ADV. See a more exact description of the data in the caption of Fig. 6.

vironmental conditions when first turning on to measure a data burst. Where alignment was not possible or was unreliable, the records were not included in the ADV and hydromast data comparison.

The recordings of water speed by the hydromasts were evaluated from the internally recorded raw data using the procedure described in Egerer et al. (2024). In laboratory and short-term field experiments, the devices were calibrated at the beginning and the end of the experiment. This procedure was not sufficient in this experiment due to the rapidly changing temperature during the measurement time. For this reason the hydromast devices were recalibrated every day to account for the temperature changes to allow more accurate velocity recordings.

The pressure recordings by hydromast H05 and the ADV (pre-processed as described) match each other almost perfectly in terms of timing, phase and magnitude of fluctuations (Fig. 6). The ADV tends to smooth out the largest values of pressure fluctuations and to provide a flatter temporal course of the pressure signal at its maxima and minima. As this

pattern persisted during most of the experiment, it may be associated with a faster reaction of the hydromast pressure sensor to pressure fluctuations. However, on some occasions (e.g. at 12:30 on 31.08) the pressure signals recorded by the two devices were in counter-phase for a few wave periods. It is likely that this reflects the presence of a few short crests or pyramidal waves that create different pressure signals at the locations of the sensors.

A comparison of the ADV data with the velocity proxy from the hydromasts shows much larger differences (Fig. 7). The timing and phase of water speed fluctuations evaluated using the two devices match each other well. However, the magnitudes of water speed fluctuations differ considerably. There is no clear bias for higher water speeds (>0.2 m/s) even though the water speed under subsequent wave crests may follow a different pattern. This feature may be to some extent caused by extensive along-crest variations of water elevation or by the presence of a pyramidal wave field.

Hydromasts have been developed for flows in the speed range of 0.15–1 m/s (Egerer et al. 2024). The reason is that
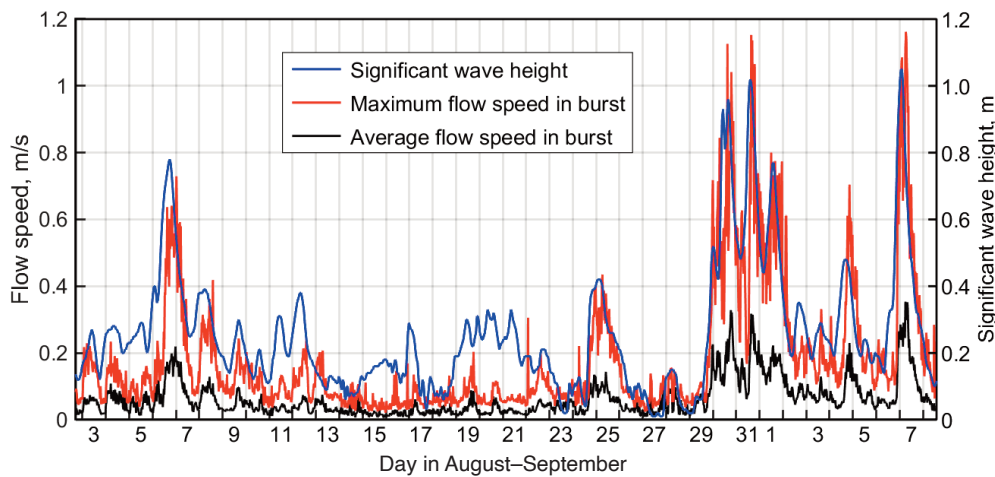
Fig. 9. Flow speed evaluated from the velocity components registered using the ADV during the experiment and significant wave height modelled near the experiment site (Fig. 2).

at flow speeds <0.1 m/s the mast is almost still, the output is almost constant and thus the estimates of flow speed are inadequate. The applicability of hydromast speed recordings in the range of 0.1–0.15 m/s is discussed in detail in Section 'Matching ADV and hydromast data'.

The flow directions evaluated using hydromasts for water speeds both below and above approximately 0.12 m/s match well with those estimated by the ADV device (Fig. 8). The match is reasonable also for a relatively low water speed (Fig. 8). This feature signals that on most occasions the flow direction is recorded adequately even when the flow speed recording is not reliable. Sharp peaks registered by the hydromast mirror very low values of water speeds when the reliability of determining flow directions is low.

Results

Flow speed

Following the variations in the significant wave height in the vicinity of the study area (Fig. 3), hydrodynamic conditions substantially varied during the experiment (Fig. 9). As mentioned above, the average horizontal flow speed was 0.0630 m/s. The water speed was on the order of 0.1 m/s or even lower at the very beginning of August and from 10 August until the end of August. A few events with maximum water speed up to 0.6 m/s occurred on 7–9 and 25 August. The registered water velocities were much higher, often 0.4 m/s and up to 1.2 m/s from 30 August and on several occasions in September. This level of intermittency of water velocities and associated hydrodynamic loads is an intrinsic feature of wave fields in the Baltic proper (Soomere and Eelsalu 2014). As waves are mostly produced locally in the Gulf of Riga (Najafzadeh et al. 2024), this feature is apparently even more pronounced in this water body.

In the linear approximation, wave-induced water speed linearly depends on the wave height (e.g. Dean and Dalrymple 1991). This feature was commonly evident during this experiment, particularly under all higher wave conditions when the waves approached from the north, northwest or west. Formally, the water speed does not follow this relationship, only during southern and south-eastern winds (Fig. 3) on 4–6, 11–12, 15–17 and 19–22 August. Winds from these directions are either blowing in the offshore direction at

Skulte or produce waves that propagate along the shore and are much lower in the nearshore because of wave energy redistribution during refraction. It is natural that on both occasions the modelled wave heights in the model grid cell at a greater distance from the shore are considerably higher than the waves at the measurement location.

The average ratio of the maximum and mean values of flow speed in single bursts is 2.83 but reaches 28 in one burst. It is likely that several single short peaks of flow speed in the recordings reflect vessel traffic to or from the Port of Skulte. The nature of such peaks on 16 August is addressed below in Section 'Time-frequency patterns of wave fields'. Similar peaks were observed on many occasions, at approximately midnight of 21/22 August and in the morning of 24 September.

The strongest wave conditions have created water speeds higher than 0.5 m/s and on some occasions even up to 1.2 m/s (Table 1). Water speeds >1 m/s are, technically, outside the measurement range of the hydromasts. Similar to the analysis of recordings slightly below the lower threshold of guaranteed validity, it is likely that the indicated maxima are still measured reliably. The maximum near-bottom speed driven by a 1 m high linear wave in ideal conditions in 4 m deep water is 0.52 m/s for a wave with a period of 4 s and 0.61 m/s for a wave with a period of 5 s. Flow speeds exceeding 1 m/s thus correspond to single waves with heights up to 2 m. Such single waves are rare when the (modelled) SWH is approximately 1 m (Fig. 9) but evidently common when the SWH is approximately 1.5 m, as suggested from the records of the SmartBuoy (Fig. 3). The low water speeds in the middle and at the end of August during very low wave conditions (SWH on the order of 0.05 m) may represent alongshore currents, as the maximum nearbed velocity of such waves with a height of 0.1 m and a period of 3 s is just 0.03 m/s.

Variability and intermittency of flow speed

Near-bottom velocities induced by ocean waves usually follow a Gaussian distribution (Sultan and Hughes 1993; You 2009; Bian et al. 2020). As mentioned above, we address separately the west-east (u-component, cross-shore) and south-north (v-component, alongshore) components of the recorded velocities. The distributions of both components over 1770 bursts are almost symmetric (Fig. 10). However, they have a considerably larger proportion of very low speeds (below
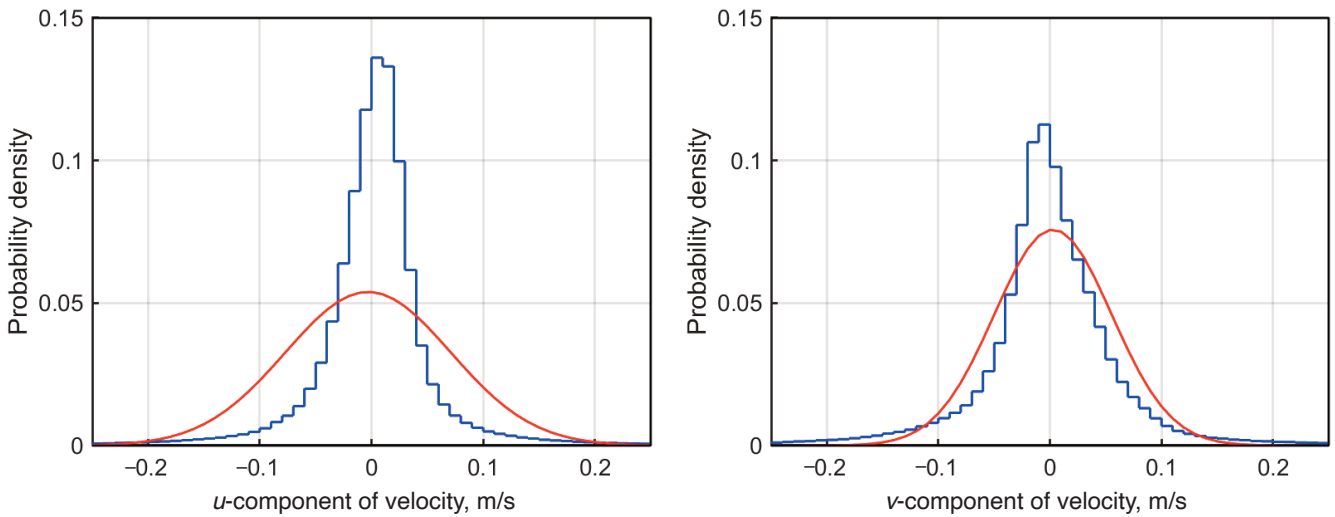
Fig. 10. Empirical distributions of the frequency of occurrence of the *u*- (west-east or cross-shore) and *v*-components (south-north or alongshore) of water velocity recorded by the ADV (stairs) and the probability density function (pdf, red line) of the associated Gaussian distributions with the same mean and variance as the measured data (μ_u = −0.0030, σ_u = 0.0740 m; μ_v = 0.0028, σ_v = 0.0526 m). The tail of the empirical distributions of the frequency of occurrence of the *u*-components is much heavier than the pdf of the associated Gaussian distribution at speeds >0.2 m/s.

0.03 m/s) than similar fields with a Gaussian distribution and a clearly smaller proportion of speeds between 0.05 and 0.1 m/s. The difference is large enough to conclude that the distributions of the recorded velocity components are not Gaussian.

An interesting feature is that both horizontal velocity components have almost zero mean values. This suggests that most of the measurement days were calm and without any considerable alongshore current at the experiment site. This feature to some extent questions the common perception of circulation in the Baltic Sea and its semi-enclosed sub-basins in terms of commonly occurring nearshore currents (Soosaar et al. 2014; Lips et al. 2016).

As the water speed induced by linear surface waves is roughly proportional to the wave height, the distribution of wave-driven flow speeds is expected to match the corresponding distribution of wave heights. The theoretical distribution of single wave heights in a narrow-banded, linear wave field is a Rayleigh distribution (Longuet-Higgins 1952). The flow speed distribution often follows a Rayleigh distribution or its direct generalisation, a two-parameter Weibull distribution (You 2009) with the shape parameter *k*, scale parameter *λ*, probability density

$$f(v) = \frac{k}{\lambda}\left(\frac{v}{\lambda}\right)^{k-1} \exp\left[-\left(\frac{v}{\lambda}\right)^k\right] \qquad (1)$$

and cumulative distribution function

$$F(v) = 1 - \exp\left[-\left(\frac{v}{\lambda}\right)^k\right]. \qquad (2)$$

The situation may be different in the case of more complicated wave fields. A Rayleigh distribution serves as a conservative upper bound for wave heights in deep water, whereas a Forristall distribution (Forristall 1978) reasonably describes individual wave heights in both long-crested and short-crested seas (Kvingedal et al. 2018). A Forristall dis-

tribution is a particular case of the Weibull distribution characterised by *k* = 2.126, while a Rayleigh distribution has *k* = 2. A Weibull distribution with *k* > 2 often reflects well individual wave heights on shallow foreshores (Battjes and Groenendijk 2000).

The Weibull distribution and its generalisations have also been commonly used to describe the distribution of significant wave heights. This quantity reflects wave properties over a certain time interval (e.g. the average of 1/3 of the highest waves recorded in 10 minutes). It thus does not necessarily reflect the distribution of individual wave heights and may require the use of more complicated generalisations of the Weibull distribution (Vanem and Fazeres-Ferradosa 2022), such as two-part distributions that separately handle moderate and severe wave conditions (Wu et al. 2016).

From a large number of studies about the appearance of the distribution of individual wave heights and wave conditions, only a few address similar distributions of water velocity in shallow water (Sultan 1992; Wiberg and Sherwood 2008; Bian et al. 2020). The above assumption that the distribution of wave-induced velocities matches the distribution of wave heights has been addressed by Xiong et al. (2020) in conditions similar to our experiment in a coastal area of the Yellow Sea. While the scale parameter varied by approximately 5% in the depth range of 0.8–27.6 m, the shape parameter was close to *k* ≈ 2 in deeper water and increased to 3–3.3 in shallow conditions. Bian et al. (2020) also demonstrated that water speeds generated by waves follow a Rayleigh distribution.

This is not the case in our experiment where the Weibull distribution of water speeds has the shape parameter *k* well below 2. The estimates of the shape parameter are *k* = 1.16 (*λ* = 0.0584), using the population-based (biased) method of moments, and *k* = 1.0633 (*λ* = 0.0648), using the Matlab built-in script for the maximum likelihood method. These two approximations do not replicate the shape of the area where
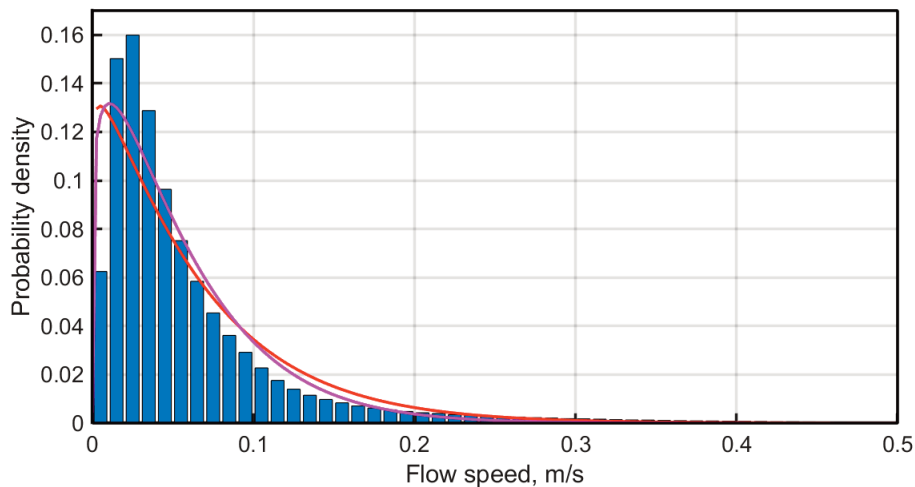
Fig. 11. Empirical probability density of water speeds evaluated from velocity components recorded by the ADV (bars) and the probability density function of the corresponding Weibull distribution with parameters estimated using the method of moments (magenta line) and the maximum likelihood method (red line). The width of speed classes is 0.1 m/s.

the most frequent waves occur in the empirical distribution (Fig. 11). The location of the mode of this distribution (close to 0.03 m/s) is greatly different from the mode of these two approximations by Weibull distributions (0.0046 m/s and 0.0106 m/s, respectively).

This empirical distribution of water speeds in our experiment is thus far from a Rayleigh distribution. Even though part of the deviation of this distribution from a Rayleigh or Weibull distribution can be explained by the presence of turbulence and currents (Bian et al. 2020), the difference is substantial. The shape of the empirical distribution of water speeds in Fig. 11 resembles typical empirical distributions of various wave conditions in semi-sheltered bays of the northern shore of Estonia (Soomere 2005). These distributions follow a Weibull distribution with a shape parameter close to one (that is, an exponential distribution) or even below one. The empirical distributions of visually estimated wave heights in the Gulf of Riga (Najafzadeh et al. 2024) have a similar appearance.

A likely reason for such an appearance of the distribution in question is a combination of the nature of the Baltic Sea wave climate and the nearshore location of the measurement site. Namely, extensive intermittence of the Baltic Sea wave climate (Soomere and Eelsalu 2014) gives rise to an unusually large proportion of low wave heights and water speeds compared to situations governed by a wave climate characterised by a Rayleigh distribution or a Weibull distribution with $k > 2$. The wave climate in the nearshore with a small proportion of remote swells has extensive time periods with very low waves generated by winds directed to the offshore. This feature additionally enhances the proportion of situations with very low waves and associated low water speeds. The infrequent presence of strong waves has limited impact on the appearance of the distribution of water speeds. The shape parameter in question changes only by about 3% if only water speeds below 0.3 m/s are considered.

**Matching ADV and hydromast data**

The above analysis has shown that the ADV data provide information about a wide range of water velocities and that this information is consistent with the existing knowledge about wave properties in the Gulf of Riga and about general properties of wave-induced motions. It is therefore acceptable

to consider the ADV recordings as the ground truth for water velocities at the site. We use this information, expressed as the relevant empirical probability density of water speed, to remove from the hydromasts' recordings the values at which the hydromast did not properly react to water motion. Doing so should not affect the distribution of the recorded higher flow speeds that are crucial for the estimates of extreme flow speeds in the area.

The typical recorded flow speeds by the ADV are well below 0.1 m/s, that is, in the range where hydromasts do not detect the flow speed (Egerer et al. 2024). It is therefore natural that the probability density function of flow speeds recorded by hydromasts has a zero value for speeds below 0.08–0.09 m/s (Fig. 12). All these inadequate recordings translate in Fig. 12 into flow speeds that are slightly higher than the threshold of flow detection. These recordings build a high and sharp spurious peak for all hydromasts around values 0.09–0.11 m/s, thus well below the threshold of formal validity of recordings 0.15 m/s in the relevant distributions. These incorrectly translated values are indistinguishable from the correct ones. Therefore, both need to be removed.

The formal validity range of the hydromast-recorded water speeds is 0.15–1 m/s (Egerer et al. 2024). As only 4.45% of the hydromast recordings are in this range (Table 1), it is desirable to include as many adequate lower speed recordings as possible into the analysis. The appearance of the probability density functions in Fig. 12 suggests that on many occasions speeds well below the threshold of 0.15 m/s are recorded correctly. These are speeds for which the relevant probability distribution matches the corresponding distribution of the ADV-recorded speeds.

For this analysis, we use empirical probability density functions of different speeds, applying 0.0025 m/s wide speed classes. A natural threshold for recordings that are most likely correct is the location in panels of Fig. 12, where the empirical probability of the ADV-recorded speeds higher than 0.1 m/s starts to match the corresponding probabilities of the hydromast-detected speeds. This location is clearly distinguishable for most of the hydromasts in Fig. 12 as a frequency at which the empirical probability of the ADV-recorded speeds becomes equal to the corresponding probability density recorded by a hydromast. This threshold varies from 0.1025 m/s for
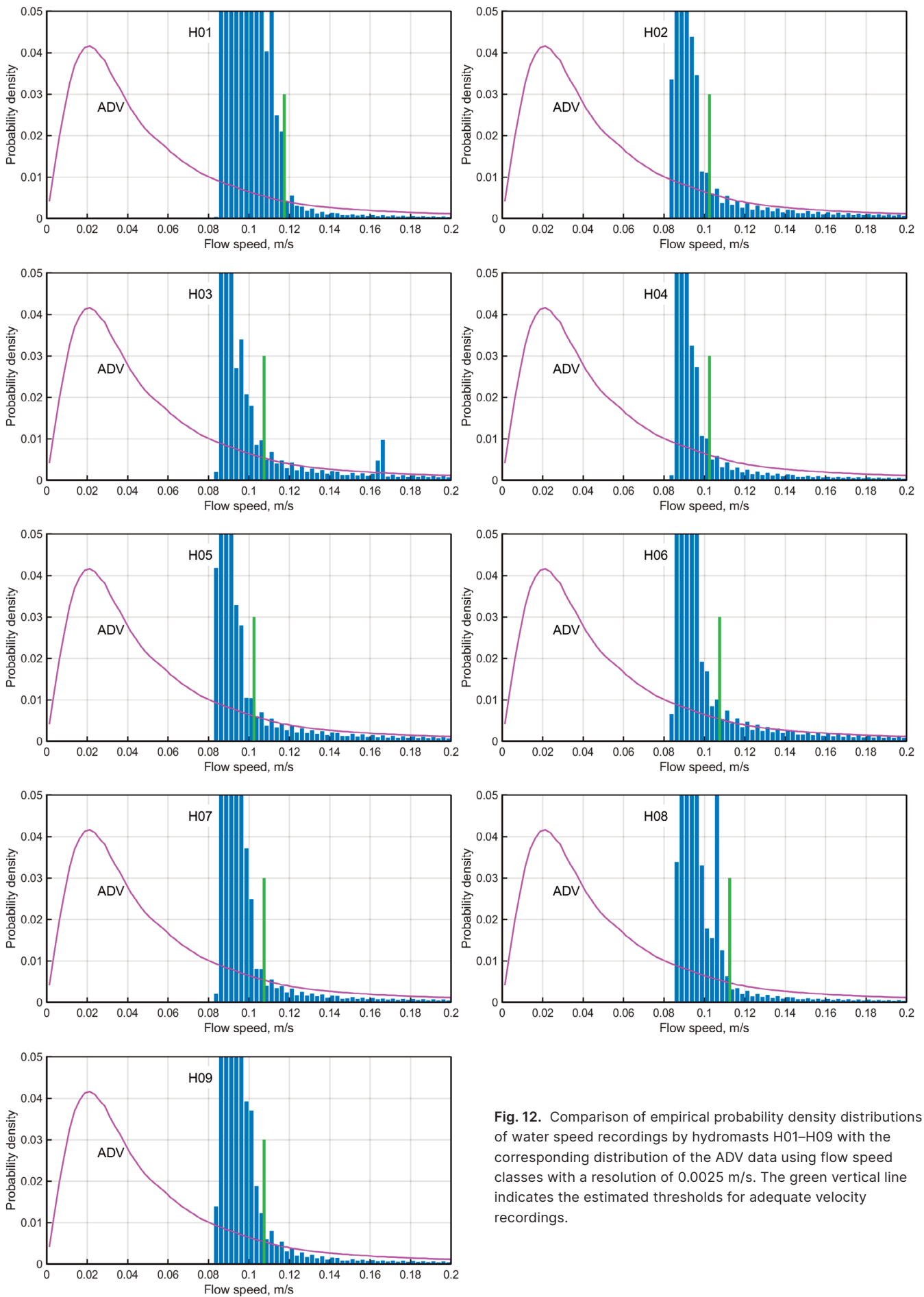
Fig. 12. Comparison of empirical probability density distributions of water speed recordings by hydromasts H01–H09 with the corresponding distribution of the ADV data using flow speed classes with a resolution of 0.0025 m/s. The green vertical line indicates the estimated thresholds for adequate velocity recordings.
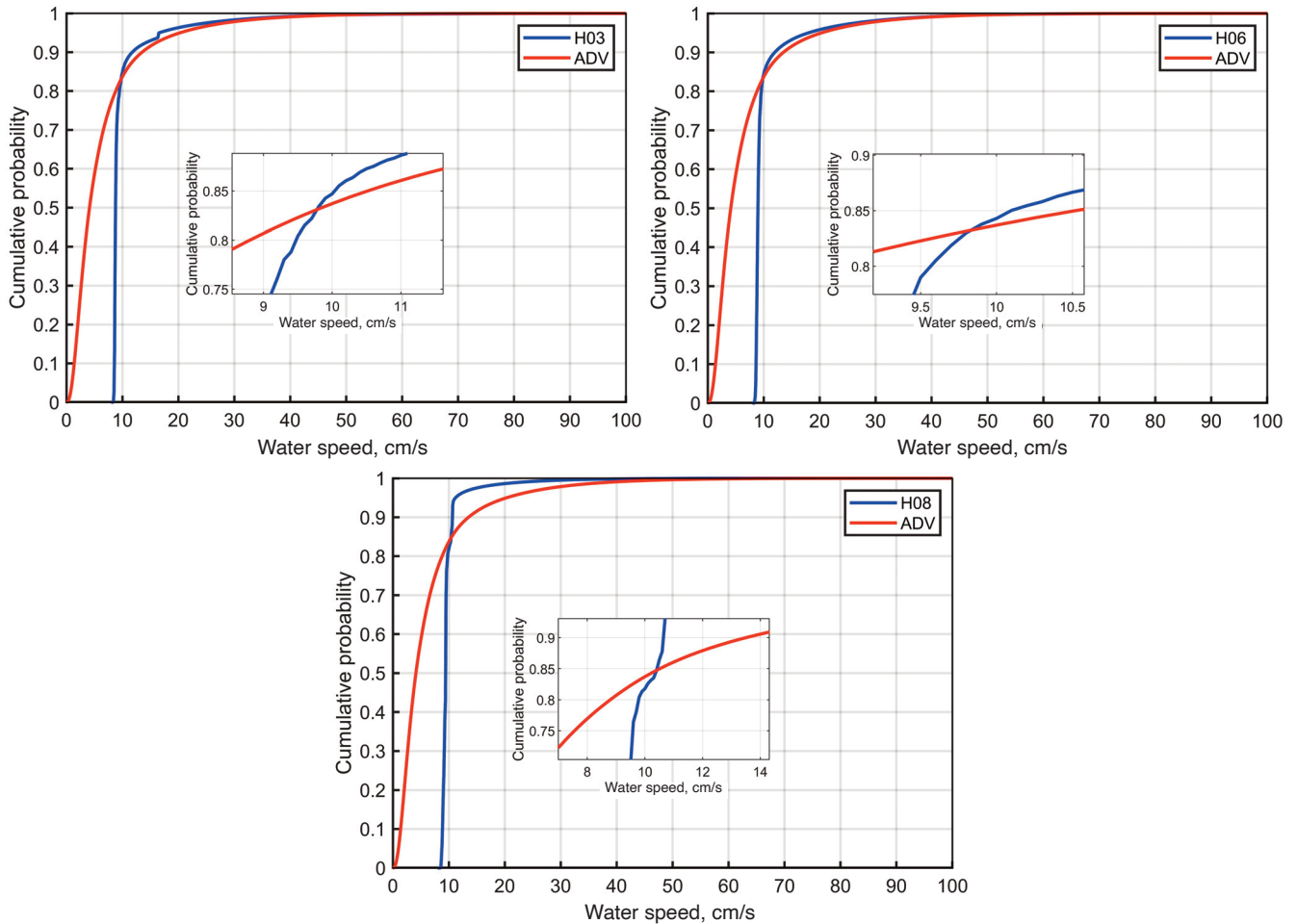
Fig. 13. Examples of cumulative probability of flow speed based on the ADV measurements and recordings of hydromasts H03, H06 and H08. The insets zoom the location of intersection of the two cumulative probabilities.

H02, H04 and H05 to 0.1175 m/s for H01 (Table 1). It is somewhat debatable whether the value 0.1075 or 0.11 should be used for H06 and H09. The use of either threshold does not have any identifiable impact on the results of the analysis. The use of such hydromast-specific or location-specific thresholds allows using 8.9% of the hydromast data. All recordings of the hydromasts below the relevant thresholds are excluded from further analysis.

The presence of large spurious peaks in Fig. 12 evidently makes it impossible to directly evaluate the full shape of the probability distributions of the hydromast-recorded water speeds. We rebuild these distributions using the assumption that the probability distribution of lower water speeds is the same at all measurement locations and represented by the distribution of the ADV-recorded speeds. Doing so enables approximations of these distributions using the Weibull distribution. The method of moments for specifying the parameters of this distribution relies exclusively on two mean values: the mean of all speed recordings and the mean of squared speed recordings. Thus, as a first approximation, we replace the mean of water speeds and their squares below the threshold for individual hydromasts by the relevant values obtained from the ADV data. Doing so most likely reduces the variability between the estimates of statistical properties of water speed in different locations. It may also to some extent affect the properties of cumulative distributions of the

hydromast-recorded water speeds. These distributions may contain discontinuity and may need renormalisation to reach the value 1 at the maximum recorded speed (Fig. 13).

Spatial variations in distributions of water speed

A very limited variation in the values of the Weibull distribution scale parameter λ for different hydromasts (Table 1) evidently reflects the procedure used for parameter estimates. For shape parameter values $k \approx 1$, the scale parameter indicates the average flow speed. As approximately 90% of the recordings used to evaluate this average are substituted by ADV recordings, it is natural that the scale parameter λ largely follows the average of the ADV-recorded speeds for all hydromasts.

The shape parameter k of this distribution is close to one on all occasions. Even though its particular values may be affected by the use of the ADV-recorded values, it is likely that water speed in the measurement location generally follows an exponential distribution with $k \approx 1$. Interestingly, the largest difference between the values of the shape parameter k of the ADV-recorded and hydromast-recorded water speeds occurs for hydromast H05 that was mounted in the proximity of the ADV device. The smaller this parameter the 'heavier' is the tail of this distribution and thus the larger the probability of encountering high speeds. Hydromast H05 systematically recorded higher water speeds than the other
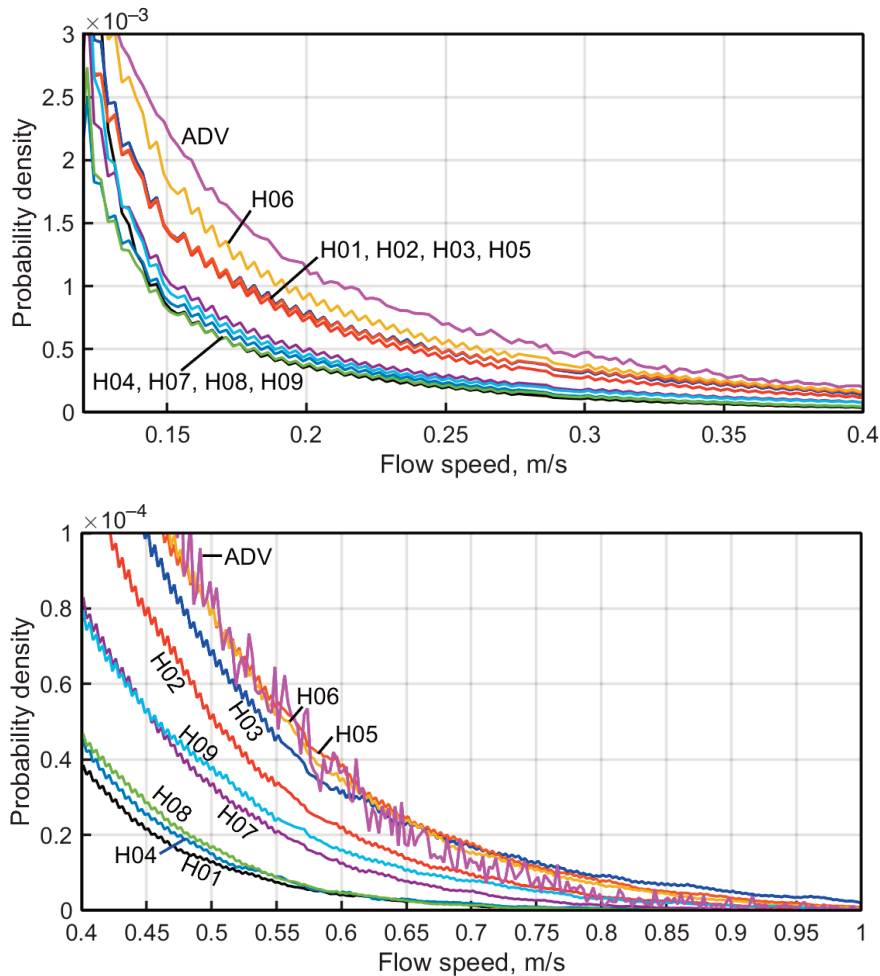
Fig. 14. Comparison of empirical probability density distributions of water speed recordings by hydromasts H01–H09 with the corresponding probability that reflects the ADV data in the range of speeds 0.15–0.4 m/s (upper panel) and 0.4–1 m/s (lower panel). The single values of probability density of the hydromast-recorded speeds with a resolution of 0.0025 m/s are smoothed over five subsequent values in the upper panel and over nine subsequent values in the lower panel.

devices, except for H06 (Table 1). It is thus unlikely that high speeds recorded by H05 result from a disturbance to the flow by the neighbouring ADV device.

The variations in the shape parameter of the Weibull distribution (Table 1) become evident in the probability differences of the hydromast-recorded speeds in the range of relatively frequently occurring speeds of 0.15–0.4 m/s (Fig. 14). The performed operations towards the identification of adequate recordings of water speeds in the hydromast data do not affect the probabilities of the occurrence of water speeds >0.15 m/s. These probabilities form three distinct groups, whereas the probabilities of the hydromast-recorded speeds are clearly smaller than the probability of the ADV-recorded speeds in the entire range. The lowest speed probabilities of this range are retrieved by hydromasts H04, H07, H08 and H09. These probabilities are approximately 50% higher in the data from hydromasts H01, H02, H03 and H05, and an additional 20% higher in the data from hydromast H06. The difference between the ADV-suggested probabilities and those retrieved by hydromasts H04, H07, H08 and H09 is approximately 2.5 times across the entire range. This variation and clustering of the relevant graphs into three groups suggests that the probabilities in question at least somewhat depend on the (calibration) properties of hydromasts. It is also possible that the described variations reflect non-linear response of the device to the changing flow speed.

The probability of the ADV-recorded higher flow speeds >0.4 m/s matches this probability for H03, H05 and H06 in the range of 0.5–0.6 m/s (Fig. 14) and becomes smaller than this probability for most of the hydromasts (except for H01, H04 and H08) for speeds >0.8 m/s. The grouping of hydromasts in terms of these probabilities is different from the above. The smallest probabilities in this range of speeds show recordings of hydromasts H01, H04 and H08. Approximately twice as large probabilities occur in the recordings of H07 and H09 and three times as large in the recordings of H02.

The maximum speed recorded by the ADV was 1.162 m/s. As usual for these kinds of measurements, the single maximum values may contain relatively large uncertainties. Even though the empirical probability of high water speeds decreases rapidly (Figs 12–14), the approximations of this distribution using Weibull distributions, with parameters evaluated using two approaches (method of moments and maximum likelihood method), underestimate the empirical probability by several orders of magnitude in the range of water speeds 0.4–0.8 m/s (Fig. 15). The underestimation is particularly severe by the version of this distribution that is constructed using the method of moments. A speed >0.51 m/s should happen less than once in single bursts based on the approximation constructed using the method of moments, and a speed >0.67 m/s should happen less than once according to the approximation constructed using the maximum likelihood method.

More information about the nature of probability distributions of flow speeds is given by the semilogarithmic display of these distributions (Fig. 16). Interestingly, the
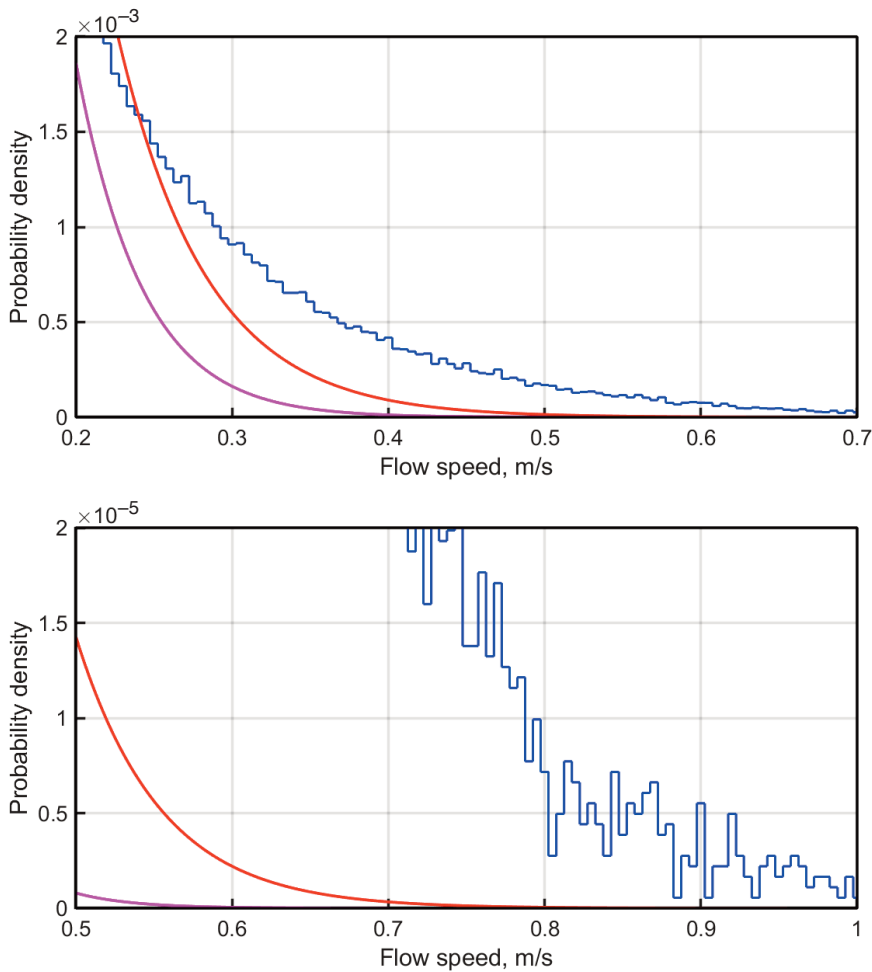
Fig. 15. Empirical probability densities of the ADV-recorded water speeds (stairs) in the range of 0.2–0.7 m/s (upper panel) and 0.5–1 m/s (lower panel). Magenta and red lines show the probability density function of the corresponding Weibull distribution with the parameters estimated using the method of moments and maximum likelihood method, respectively. The width of speed classes is 0.005 m/s. The probability of occurrence of one event (5.5×10^{-7}) is first reached at 0.885 m/s.
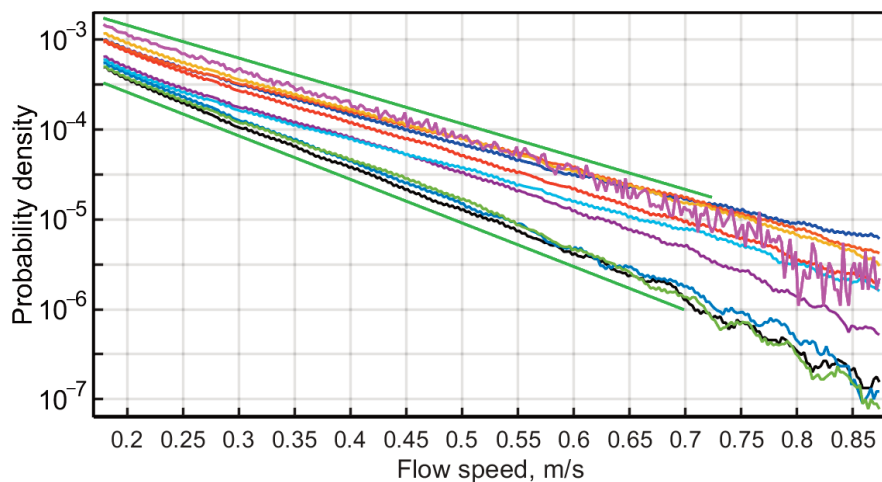
logarithms of empirical probability densities almost perfectly follow straight lines in a large range of recorded speeds. This feature means that all these probability distributions follow the same type of exponential distribution $f(v) = A\exp(-Av)$ with different values of the rate parameter A. This distribution is a particular case of the Weibull distribution when $k = 1$:

$$f(v) = \frac{1}{\lambda}\exp\left(-\frac{v}{\lambda}\right). \qquad (3)$$

The slope of the relevant lines for hydromasts H01–H09 ($-A$ in this notion) varies from –7.08 (H03) to –12.2 (H08) in the range of 0.25–0.875 m/s (Table 1). These values are by a factor of 2–2.5 higher than the estimates of these slopes $A = 1/\lambda$, based on the values of λ in Table 1. It is likely that

this mismatch stems from the substitution of statistical properties of the hydromast data below the threshold in Table 1 by the corresponding properties of the ADV data. Namely, the average flow speed in these conditions when the flow speed regularly exceeded the thresholds in Table 1 would obviously be higher than the average of the ADV-recorded water speed during the entire experiment.

The presented material suggests that all empirical probability distributions of higher water speeds recorded by hydromasts have the same basic shape of exponential distribution, equivalently, a Weibull distribution with $k = 1$. The presence of this type of distribution matches similar distributions for wave heights in the nearshore of the sheltered Tallinn Bay on the northern shore of Estonia (Soomere 2005). Even

Fig. 16. Empirical probability densities of recorded water speeds in the range of 0.18–0.875 m/s in semilogarithmic coordinates. Colour code of probability densities for H01–H09 is the same as in Fig. 15. Green straight lines match the slope of the uppermost and lowermost lines for the hydromasts.
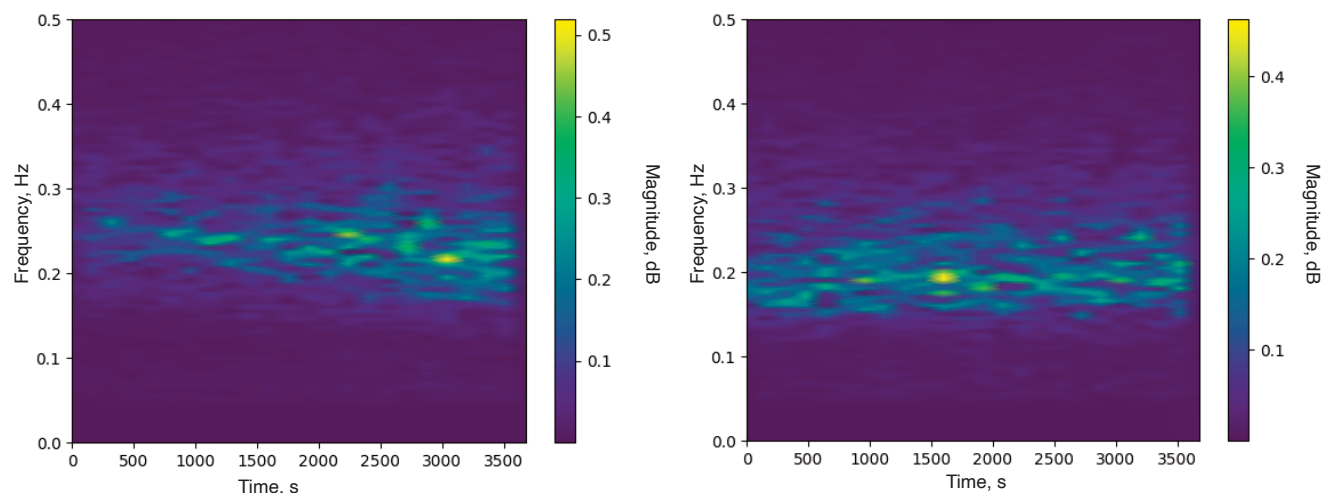
Fig. 17. Time-frequency 'portraits' of an approaching wave storm at 13:00–14:00 EEST on 31 August 2022 (left panel) and wave conditions during the final stage of a wave storm at 22:00–23:00 EEST on 31 August 2022 (right panel), registered by the pressure sensor of hydromast H05. The modelled wave height (Fig. 3) increased at 13:00–14:00 from 0.93 m to 1 m, reaching a maximum of 1.02 m at 15:00 while the peak period was 5.17 s and waves approached from the north-west (314–315°). The modelled wave height decreased at 22:00–23:00 from 0.68 m to 0.62 m, while the peak period decreased from 5.69 s at 21:00 to 5.17 s at 22:00–23:00, and waves approached from the same direction.

though single devices may have slightly different characteristics that may to some extent affect this shape, it is likely that the described differences in these distributions reflect spatial variability in the near-seabed flow field.

Time-frequency patterns of wave fields

The ability of hydromasts to perform continuous long-term high-resolution recordings of local flow properties opens the way for a variety of applications where the changes in the flow speed or direction, or other affected hydrodynamic variables, such as pressure, carry crucial information. A simple application is the detailed time-frequency portrait of wave storms in the area, presented as spectrograms of recorded time series of pressure (Fig. 17). An approaching or developing wave storm starts from a wave system with a peak period around 3 s (Fig. 17, left panel). Over time, more energy is added to the wave field as indicated by the 'greening' of the time-frequency diagram. This process is accompanied by a gradual increase in the peak wave period that reaches 5–6 s at the end of the record. When a wave storm is ceasing (Fig. 17, right panel), the energy that is originally spread over a wide range of periods is becoming gradually concentrated in a narrow range of periods around 5 s. This representation carries much more information than the classic integrated wave properties or two-dimensional wave spectra. As wind direction often changes during the storm, the ability of hydromasts to also record flow direction can be used for even more detailed portraying of the properties and course of the wave storm.

A more detailed application of this kind of 'portrait' of wave patterns can be used to identify signals from various vessels that sail in the vicinity of the measurement site during relatively calm conditions (Rätsep et al. 2021). These signals have a clear pattern in the time-frequency domain that usually consist of two branches in the spectrograms. While the narrow-angle structure on the left panel of Fig. 18 is apparently produced by a vessel that sails at a relatively low speed and

creates a basically linear Kelvin wake, the L-like feature on the right panel of Fig. 18 likely mirrors a passage of a rapidly moving vessel that produced a large number of nonlinear disturbances (Torsvik et al. 2015; Rätsep et al. 2020). Similar to the above-described example, the exact flow speeds are less important, and the core benefit comes from the ability to rapidly react to changing flow speed and to provide adequate information about changing the properties of the signal. An additional benefit may be obtained from several synchronised recordings that can be used to highlight the useful signal and suppress the background of natural waves (Rätsep et al. 2020). Moreover, the information about the wave-induced flow direction considerably simplifies the task of evaluating the ship's course from wake recordings (Rätsep et al. 2021).

Discussion

The experiments were performed in approximately 4 m deep water, that is, well offshore from the breaker line, with single waves up to 2 m high during the campaign. The flow speed measurements reflect water velocities at an average height of 0.4–0.45 m above the seabed. The common values of the thickness of the wave bottom boundary layer are well below 10 cm (Trowbridge and Lentz 2018), as was also established by high-resolution measurements in approximately 2 m (Foster et al. 2000) and 3.7 m deep water (Zou and Hay 2003). Therefore, the height of the measurement points of the used devices is generally well above the bottom boundary layer. The results thus provide an estimate of water speed that well reflects the local wave properties and can directly be used for estimates of wave-driven seabed stresses for various purposes, including entrainment of finer sediment into flow and specification of thresholds for initiation of sediment motion (Pähtz et al. 2020).

The presence of very low residual currents at the experiment site is, to a certain extent, intriguing, as the common
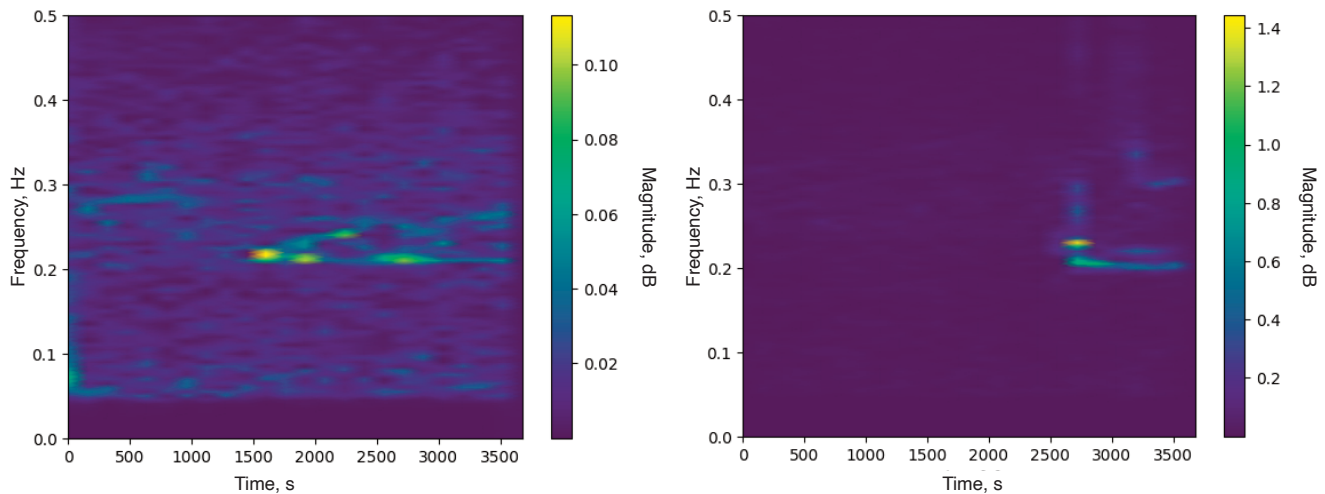
Fig. 18. Time-frequency 'portraits' of the wake of a slow vessel passing the experiment site at 04:00–05:00 EEST on 16 August 2022 (left panel) and a signature that likely reflects the passing of a rapidly sailing vessel at 17:00–18:00 EEST on 16 August 2022 (right panel), registered by the pressure sensor of hydromast H05. The modelled wave height was 0.16 m at 04:00–05:00, the peak period varied from 1.62 to 1.79 s and waves approached from the south-east (140°). The wave height was even lower (0.13–0.14 m) and the peak period even shorter (1.47–1.62 s) at 17:00–18:00, and waves approached from the east-south-east (103–106°). As on both occasions the wind blew from the Latvian mainland to the offshore, it is likely that the predominant wave heights and periods were even smaller at the measurement location.

perception of the dynamics of the Gulf of Riga involves a system of coastal currents (see e.g. Soosaar et al. 2014; Lips et al. 2016). On the one hand, it seems that the open-sea currents do not penetrate into the nearshore. On the other hand, this feature signals that the wave-driven alongshore currents are concentrated at smaller depths and closer to the shore than the measurement location. The combination of these two features makes the 'intermediate' site, slightly onshore from the location of closure depth, a promising place for recording and detecting ship passages as well as for assessing their impact on the shore.

The analysis of the recordings of relatively low speeds (below 0.15 m/s) reveals the variations in how different hydromasts record flow speed. Even though the proven range of recorded speeds is from 0.15 m/s (Egerer et al. 2024), all devices seem to record flow speeds adequately from 0.12 m/s, while several devices provide reliable output starting from the flow speeds of 0.1 m/s. This expansion of the range of validity not only increases the pool of adequate recordings by a factor of two but also makes it possible to analyse the probability distributions of wave-induced speeds over a much wider range.

The analysis of the ADV-recorded water speeds reveals that classic distributions for wave-driven flow speed, such as the Weibull distribution, underestimate the probability of occurrence of wave-induced flow speed starting from approximately 0.25 m/s, that is, for the motions that are almost definitely driven by surface waves at the study area, where we have not detected any strong coastal current. They underestimate this probability by several orders of magnitude for relatively frequently occurring speeds of 0.5–0.7 m/s. This underestimation is most likely a general feature of the hydrodynamic fields at the experiment site rather than a local anomaly. This feature may translate to an equally severe underestimation of the impact of waves on bottom sediments and the underwater parts of various structures.

Most importantly, the empirical probability distributions of the recorded flow speeds definitely do not follow the classic Rayleigh or Forristall distributions that are commonly applied to describe distributions of wave heights and wave-induced water speed on open ocean beaches. As the Rayleigh distribution is based on theoretical arguments that do not necessarily hold for surface waves in real oceans and seas, it is not very surprising that it does not become evident in our analysis. The Forristall distribution is an empirically established distribution. One might thus expect it to work better. However, all empirical probability distributions of flow speeds recorded by the ADV and hydromasts are even more different from a Forristall distribution than from a Rayleigh distribution. They all almost perfectly follow an exponential distribution for a wide range of speeds, from the level close to the reliable detection threshold (0.15 m/s) up to values that are approximately 80% of the maximum speed recorded by each device. The presence of this kind of distribution seems to be characteristic of the local, extremely intermittent nearshore wave climate, similar to the one in North Estonian bays (Soomere 2005), where wave heights are very low during long time periods when winds blow from the mainland to the offshore.

It is likely that the presence of short-crested waves enhances spatial variations in the wave-driven flow properties and resulting loads on the seabed and structures (Zheng et al. 2006). We tested this assumption to a first approximation by addressing the spatial variability of the properties of empirical flow speed distributions. The above-described differences in the threshold for reliably recorded flow speeds do not impact the basic shape of the relevant empirical probability distributions even though they may slightly affect some parameters of these distributions. The exponent (rate parameter) of the established exponential distribution varies by almost two times for different devices. This parameter for the ADV-recorded speeds is within the range of the rate parameters for

the set of the hydromasts. This variation obviously reflects, to some extent, differences in the properties of custom-built devices used in experiments. However, it most likely also mirrors, at least to some extent, variations in the properties of the wave-driven nearbed flow pattern in the measurement site. A more exact quantification of these variations is apparently possible by using a set of devices that are calibrated so that the recorded empirical probability distributions of flow speeds are identical.

Conclusions

A very weak residual current was detected at the study site, signalling that the offshore circulation in the Gulf of Riga does not penetrate to a depth of 4 m. The distributions of the components of water velocity are symmetric but substantially deviate from a Gaussian distribution that is commonly used to characterise these velocities on open ocean shores.

The empirical distribution of the occurrence of different flow speeds is remarkably different from the commonly used Rayleigh or Forristall distributions for wave heights and wave-induced velocities. The Weibull distribution severely underestimates the probability of the occurrence of higher water speeds above 0.3 m/s.

The distributions of measured water speeds follow an exponential distribution, equivalently, a Weibull distribution with a shape parameter close to one, for all devices. It is likely that this distribution is characteristic of wave heights and wave-induced flow speeds in relatively sheltered coastal areas with a low proportion of swells.

Data availability statement

The recorded data sets are available by request from the authors: the hydromast data from the contributors from the Centre of Biorobotics and the ADV data from K. Parnell.

Acknowledgements

References

Aagaard, T., Brinkkemper, J., Christensen, D. F., Hughes, M. G. and Ruessink, G. 2021. Surf zone turbulence and suspended sediment dynamics – a review. *J. Mar. Sci. Eng.*, **9**(11), 1300. https://doi.org/10.3390/jmse9111300

Battjes, J. A. and Groenendijk, H. W. 2000. Wave height distributions on shallow foreshores. *Coast. Eng.*, **40**(3), 161–182. https://doi.org/10.1016/S0378-3839(00)00007-7

Bian, C., Liu, X., Zhou, Z., Chen, Z., Wang, T. and Gu, Y. 2020. Calculation of winds induced bottom wave orbital velocity using the empirical mode decomposition method. *J. Atmos. Ocean. Technol.*, **37**(5), 889–900. https://doi.org/10.1175/JTECH-D-19-0185.1

Björkqvist, J.-V., Lukas, I., Alari, V., Vledder, G. P. V., Hulst, S., Pettersson, H. et al. 2018. Comparing a 41-year model hindcast with decades of wave measurements from the Baltic Sea. *Ocean Eng.*, **152**, 57–71. https://doi.org/10.1016/j.oceaneng.2018.01.048

Björkqvist, J.-V., Pärt, S., Alari, V., Rikka, S., Lindgren, E. and Tuomi, L. 2021. Swell hindcast statistics for the Baltic Sea. *Ocean Sci.*, **17**, 1815–1829. https://doi.org/10.5194/os-17-1815-2021

Bleckmann, H. and Zelick, R. 2009. Lateral line system of fish. *Integr. Zool.*, **4**(1), 13–25. https://doi.org/10.1111/j.1749-4877.2008.00131.x

Broman, B., Hammarklint, T., Rannat, K., Soomere, T. and Valdmann, A. 2006. Trends and extremes of wave fields in the north-eastern part of the Baltic Proper. *Oceanologia*, **48**, 165–184.

Bullock, G. N., Obhrai, C., Peregrine, D. H. and Bredmose, H. 2007. Violent breaking wave impacts. Part 1: results from large-scale regular wave tests on vertical and sloping walls. *Coast. Eng.*, **54**(8), 602–617. https://doi.org/10.1016/j.coastaleng.2006.12.002

Christensen, D. F., Hughes, M. G. and Aagaard, T. 2019. Wave period and grain size controls on short-wave suspended sediment transport under shoaling and breaking waves. *J. Geophys. Res. Earth Surf.*, **124**(12), 3124–3142. https://doi.org/10.1029/2019JF005168

Coles, S. 2004. *An Introduction to Statistical Modeling of Extreme Values*. 3rd ed. Springer, London.

Dean, R. G. and Dalrymple, R. A. 1991. *Water Wave Mechanics for Engineers and Scientists*. World Scientific, Portland.

Diplas, P., Dancey, C. L., Celik, A. O., Valyrakis, M., Greer, K. and Akar, T. 2008. The role of impulse on the initiation of particle movement under turbulent flow conditions. *Science*, **322**(5902), 717–720. https://doi.org/10.1126/science.1158954

Eelsalu, M., Org, M. and Soomere, T. 2014. Visually observed wave climate in the Gulf of Riga. In *2014 IEEE/OES Baltic International Symposium (BALTIC), Tallinn, Estonia, 27–29 May 2014*. IEEE, 1–10. https://doi.org/10.1109/BALTIC.2014.6887829

Egerer, M., Ristolainen, A., Piho, L., Vihman, L. and Kruusmaa, M. 2024. Hall effect sensor-based low-cost flow monitoring device: design and validation. *IEEE Sens. J.*, **24**(5), 5986–5997. https://doi.org/10.1109/JSEN.2024.3354194

Forristall, G. Z. 1978. On the statistical distributions of wave heights in a storm. *J. Geophys. Res. Oceans*, **83**(C5), 2353–2358. https://doi.org/10.1029/JC083iC05p02353

Foster, D. L., Beach, R. A. and Holman, R. A. 2000. Field observations of the wave bottom boundary layer. *J. Geophys. Res. Oceans*, **105**(C8), 19631–19647. https://doi.org/10.1029/1999JC900018

Giudici, A., Jankowski, M. Z., Männikus, R., Najafzadeh, F., Suursaar, Ü. and Soomere, T. 2023. A comparison of Baltic Sea wave properties simulated using two modelled wind data sets. *Estuar. Coast. Shelf Sci.*, **290**, 108401. https://doi.org/10.1016/j.ecss.2023.108401

Huang, N. E., Sheng, Z., Long, S. R., Wu, M. C., Shih, H. H., Zheng, Q. et al. 1998. The empirical mode decomposition and the Hilbert spectrum for nonlinear and nonstationary time series analysis. *Proc. R. Soc. Lond. A.*, **454**(1971), 903–995. https://doi.org/10.1098/rspa.1998.0193

Kvingedal, B., Bruserud, K. and Nygaard, E. 2018. Individual wave height and wave crest distributions based on field measurements from the northern North Sea. *Ocean Dyn.*, **68**(12), 1727–1738. https://doi.org/10.1007/s10236-018-1216-y

Leppäranta, M. and Myrberg, K. 2009. *Physical Oceanography of the Baltic Sea*. Springer, Berlin, Heidelberg. https://doi.org/10.1007/978-3-540-79703-6

Lips, U., Zhurbas, V., Skudra, M. and Väli, G. 2016. A numerical study of circulation in the Gulf of Riga, Baltic Sea. Part I: whole-basin gyres and mean currents. *Cont. Shelf Res.*, **112**, 1–13. https://doi.org/10.1016/j.csr.2015.11.008

Longuet-Higgins, M. S. 1952. On the statistical distribution of heights of sea waves. *J. Mar. Res.*, **11**(3), 245–266.

Ma, Y., Tai, B., Xie, B., Xu, T., Perlin, M. and Dong, G. 2023. Progress in the research of wave slamming forces on vertical cylinders. *J. Mar. Sci. Appl.*, **22**(1), 1–13. https://doi.org/10.1007/s11804-023-00313-1

Männikus, R. and Soomere, T. 2023. Directional variation of return periods of water level extremes in Moonsund and in the Gulf of Riga, Baltic Sea. *Reg. Stud. Mar. Sci.*, **57**, 102741. https://doi.org/10.1016/j.rsma.2022.102741

Najafzadeh, F., Jankowski, M. Z., Giudici, A., Männikus, R., Suursaar, Ü., Viška, M. et al. 2024. Spatiotemporal variability of wave climate in the Gulf of Riga. *Oceanologia*, **66**(1), 56–77. https://doi.org/10.1016/j.oceano.2023.11.001

Pähtz, T., Clark, A. H., Valyrakis, M. and Durán, O. 2020. The physics of sediment transport initiation, cessation, and entrainment across aeolian and fluvial environments. *Rev. Geophys.*, **58**(1), e2019RG000679. https://doi.org/10.1029/2019RG000679

Poncet, P. A., Liquet, B., Larroque, B., D'Amico, D., Sous, D. and Abadie, S. 2022. In-situ measurements of energetic depth-limited wave loading. *Appl. Ocean Res.*, **125**, 103216. https://doi.org/10.1016/j.apor.2022.103216

Rätsep, M., Parnell, K. E., Soomere, T., Kruusmaa, M., Ristolainen, A. and Tuhtan, J. A. 2020. Using spectrograms from underwater total pressure sensors to detect passing vessels in a coastal environment. *J. Atmos. Ocean. Technol.*, **37**(8), 1353–1363. https://doi.org/10.1175/JTECH-D-19-0192.1

Rätsep, M., Parnell, K. E., Soomere, T., Kruusmaa, M., Ristolainen, A. and Tuhtan, J. A. 2021. Surface vessel localization from wake measurements using an array of pressure sensors in the littoral zone. *Ocean Eng.*, **233**, 109156. https://doi.org/10.1016/j.oceaneng.2021.109156

Ristolainen, A., Tuhtan, J. A., Kuusik, A. and Kruusmaa, M. 2016. Hydromast: a bioinspired flow sensor with accelerometer. In *Biomimetic and Biohybrid Systems. Living Machines 2016. Lecture Notes in Computer Science* (Lepora, N., Mura, A., Mangan, M., Verschure, P., Desmulliez, M. and Prescott, T., eds). Springer, Cham, **9793**, 510–517. https://doi.org/10.1007/978-3-319-42417-0_55

Ristolainen, A., Tuhtan, J. A. and Kruusmaa, M. 2019. Continuous, near-bed current velocity estimation using pressure and inertial sensing. *IEEE Sens. J.*, **19**(24), 12398–12406. https://doi.org/10.1109/JSEN.2019.2937954

Soomere, T. 2003. Anisotropy of wind and wave regimes in the Baltic Proper. *J. Sea Res.*, **49**(4), 305–316. https://doi.org/10.1016/S1385-1101(03)00034-0

Soomere, T. 2005. Wind wave statistics in Tallinn Bay. *Boreal Env. Res.*, **10**(2), 103–118. http://www.borenv.net/BER/archive/pdfs/ber10/ber10-103.pdf

Soomere, T. and Eelsalu, M. 2014. On the wave energy potential along the eastern Baltic Sea coast. *Renew. Energ.*, **71**, 221–233. https://doi.org/10.1016/j.renene.2014.05.025

Soomere, T., Männikus, R., Pindsoo, K., Kudryavtseva, N. and Eelsalu, M. 2017. Modification of closure depths by synchronisation of severe seas and high water levels. *Geo-Mar. Lett.*, **37**(1), 35–46. https://doi.org/10.1007/s00367-016-0471-5

Soosaar, E., Maljutenko, I., Raudsepp, U. and Elken, J. 2014. An investigation of anticyclonic circulation in the southern Gulf of Riga during the spring period. *Cont. Shelf Res.*, **78**, 75–84. https://doi.org/10.1016/j.csr.2014.02.009

Sultan, N. J. 1992. *Irregular wave-induced velocities in shallow water*. Technical report CERC-92-9. US Army Corps of Engineers, Washington DC.

Sultan, N. J. and Hughes, S. A. 1993. Irregular wave-induced velocities in shallow water. *J. Waterw. Port Coast. Ocean Eng.*, **119**(4), 429–447. https://doi.org/10.1061/(ASCE)0733-950X(1993)119:4(429)

Suursaar, Ü., Kullas, T. and Otsmann, M. 2002. A model study of the sea level variations in the Gulf of Riga and the Väinameri Sea. *Cont. Shelf Res.*, **22**(14), 2001–2019. https://doi.org/10.1016/S0278-4343(02)00046-8

Torsvik, T., Soomere, T., Didenkulova, I. and Sheremet, A. 2015. Identification of ship wake structures by a time-frequency method. *J. Fluid Mech.*, **765**, 229–251. https://doi.org/10.1017/jfm.2014.734

Trowbridge, J. H. and Lentz, S. J. 2018. The bottom boundary layer. *Ann. Rev. Mar. Sci.*, **10**, 397–420. https://doi.org/10.1146/annurev-marine-121916-063351

Vanem, E. and Fazeres-Ferradosa, T. 2022. A truncated, translated Weibull distribution for shallow water sea states. *Coast. Eng.*, **172**, 104077. https://doi.org/10.1016/j.coastaleng.2021.104077

Viška, M. and Soomere, T. 2013. Simulated and observed reversals of wave-driven alongshore sediment transport at the eastern Baltic Sea coast. *Baltica*, **26**(2), 145–156. https://doi.org/10.5200/baltica.2013.26.15

Wiberg, P. L. and Sherwood, C. R. 2008. Calculating wave-generated bottom orbital velocities from surface-wave parameters. *Comput. Geosci.*, **34**(10), 1243–1262. https://doi.org/10.1016/j.cageo.2008.02.010

Wu, Y., Randell, D., Christou, M., Ewans, K. and Jonathan, P. 2016. On the distribution of wave height in shallow water. *Coast. Eng.*, **111**, 39–49. https://doi.org/10.1016/j.coastaleng.2016.01.015

Xiong, J., You, Z.-J., Li, J., Gao, S., Wang, Q. and Wang, Y. P. 2020. Variations of wave parameter statistics as influenced by water depth in coastal and inner shelf areas. *Coast. Eng.*, **159**, 103714. https://doi.org/10.1016/j.coastaleng.2020.103714

You, Z.-J. 2009. The statistical distribution of nearbed wave orbital velocity in intermediate coastal water depth. *Coast. Eng.*, **56**(8), 844–852. https://doi.org/10.1016/j.coastaleng.2009.04.005

Zhai, Z., Li, X. and Yang, L. 2022. Analytical approach to the solution of short-crested wave interaction with V-shaped and arc-shaped breakwaters. *Phys. Fluids*, **34**(2), 022112. https://doi.org/10.1063/5.0078604

Zheng, J. H., Qian, J., Zhong, H. S. and Guo, D. 2006. Three-dimensional physical study on wave characteristics in front of concave breakwaters. In *Proceedings of the Second Sino-German Joint Symposium on Coastal and Ocean Engineering* (Yixin, Y., ed.)*, Nanjing, China, 11–20 October 2004*. China Ocean Press, 100–106.

Zou, Q. and Hay, A. E. 2003. The vertical structure of the wave bottom boundary layer over a sloping bed: theory and field measurements. *J. Phys. Oceanogr.*, **33**(7), 1380–1400. https://doi.org/10.1175/1520-0485(2003)033<1380:TVSOTW>2.0.CO;2

Liivi lahe idaranniku madalmeres järgib tuulelainete tekitatud põhjalähedaste veekiiruste tõenäosusjaotus klassikalist eksponentsiaaljaotust

Maris Eelsalu, Laura Piho, Juris Aigars, Loreta Kelpšaitė-Rimkienė, Vitalijus Kondrat, Maarja Kruusmaa, Kevin E. Parnell, Asko Ristolainen, Ilona Šakurova, Māris Skudra, Maija Viška ja Tarmo Soomere

Meie meres tekivad tavaliselt lühikeste, lühikeseharjaliste ja sageli eri suundades levivatest komponentidest koosnevad tuulelainete süsteemid. Selliste lainete tekitatud surve merepõhjale muutub ajas kiiresti ja erineb isegi lähestikku paiknevates kohtades. Kirjeldame seda muutlikkust põhjalähedaste veekiiruste kaudu. Kiiruseid mõõdeti kaht tüüpi kõrglahutusega seadmetega Skulte sadama lähistel Lätis Liivi lahe edelarannikul 2022. a. augustis ja septembris. Üheksa uudset seadet, nn hüdromasti, paigutati kümnemeetriste vahedega 20 × 20 m mõõtmetega jäigale raamile ligikaudu 4 m sügavusse vette 700 m kaugusele rannast. Hüdromastid salvestasid rõhu hetkväärtused ning veekiiruse ja -suuna 50 korda sekundis, registreerides adekvaatselt horisontaalsed veekiirused vahemikus ligikaudu 0.12–1 m/s. Raami keskele paigutati akustiline Doppleri hoovusemõõtja, mis registreeris kiiruse kõik kolm komponenti. Ilmnes, et keskmine veekiirus rohkem kui viie mõõtmisnädala vältel oli 0.003 m/s, kusjuures maksimaalne hetkeline kiirus oli 1.22 m/s; teisisõnu, uuringukohas praktiliselt puuduvad süstemaatilised hoovused. Kiiruse horisontaalkomponentide empiiriline tõenäosusjaotus oli sümmeetriline, kuid oluliselt erinev oodatud normaaljaotusest. Hüdromastide registreeritud kiiruse absoluutväärtuste empiiriline tõenäosusjaotus järgis klassikalist eksponentsiaaljaotust, seejuures kõige paremini vahemikus 0.2–0.7 m/s, ent mitte oodatud Rayleigh või Forristalli jaotusi, mis tavaliselt seda suurust iseloomustavad. Eri seadmete registreeritud andmete põhjal hinnatud eksponentsiaaljaotuse skaalaparameetri väärtused erinesid kuni kaks korda. Ühe rakendusvõimalusena näidati, et rõhu salvestustest saab eristada Skulte sadamasse siirduvate või sealt väljuvate laevade laineid.